"Combustion Mechanism and Unsteady Burn-Rate Predictions Of New Modern Polymer-Oxidizer Mixtures"

Final Technical Report (item 0004)
by
Anatoli A. Zenin

November, 2004

United States Army

EUROPEAN RESEARCH OFFICE OF THE U.S. ARMY

London, England

CONTRACT NUMBER N62558-03-M-0812

Russian Academy of Sciences,
Semenov Institute of Chemical Physics

REPORT DOCUMENTATION PAGE			Form Approved OMB No. 0704-0188
1. AGENCY USE ONLY	2. REPORT DATE **18 November 2004**	3. REPORT TYPE AND DATES COVERED **Final Report: 18 September 2003 - 18 November 2004**	
4. TITLE AND SUBTITLE **"Combustion Mechanism and Unsteady Burn-Rate Predictions of New Modern Polymer-Oxidizer Mixtures"**			5. FUNDING NUMBERS C
6. AUTHOR **Anatoli A. Zenin**			
7. PERFORMING ORGANISATION NAME AND ADDRESS **Semenov Institute of Chemical Physics**, Russian Academy of Sciences Kosygin Street 4, 119991 Moscow, Russia			8.PERFORMING ORGANISATION REPORT NUMBER -
9. SPONSORING/MONITORING AGENCY NAME AND ADDRESS **Mr. KEVIN LINDEN** U.S. Naval Regional Contracting Center, Det. London, Government Buildings, Block 2, Wing 12, Lime Grove, Ruislip, Middlesex HA4 8BS England Telephone: 4 (0)208 385 5390; Fax: 4 (0)208 385 5348; E-mail: KEVIN.LINDEN@NRCC-LONDON.NAVY.MIL			10. SPONSORING/MONITORING AGENCY REPORT NUMBER
11. SUPPLEMENTARY NOTES			
12a. DISTRIBUTION/AVAILABILITY STATEMENT			12b. DISTRIBUTION CODE

13. ABSTRACT

Fundamental investigations of physico-chemical mechanisms of combustion were performed for new mixtures of HNIW (2,4,6,8,10,12-hexanitrohexaazaisowurtzitane) and HMX with modern energetic binders (AMMO-BAMO)+burn-rate modifier and (BAMO-THF). Burning wave structures, burning rates and main burning wave parameters were received by experiments and processing. Leading stages and macrokinetics of gasification of solid phase were established. Main features of the combustion mechanisms of the mixtures were formulated. A closed system of predictions of erosive and pulsating burning rates, typical for rocket motors, was created. The system includes obtaining: erosive burning rates, burn-rate response functions on pressure and gas velocity pulsations. The obtained corps of the characteristics describes burning rate behavior of the mixtures inside rocket chamber. Conclusions were made about combustion mechanisms of the studied mixtures under stable and pulsating external conditions, and recommendations.

14. SUBJECT ITEMS	15. NUMBER OF PAGES
Combustion mechanisms, steady and pulsating combustion, oxidizers CL-20 (HNIW), HMX, active binders, burn-rate modifier, mixtures, pressures, temperature profiles, parameters of burning waves, heat manifestations in zones, limiting stages, macrokinetics of gasification, pressure and temperature sensitivities, pressure and hot gas velocity pulsations, response functions, imitation of rocket chamber conditions.	54
	16. PRICE CODE NTIS

17. SECURITY CLASSIFICATION OF REPORT	18. SECURITY CLASSIFICATION OF THIS PAGE	19 SECURITY CLASSIFICATION OF ABSTRACT	20. LIMITATION OF ABSTRACT
UNCLASSIFIED	UNCLASSIFIED	UNCLASSIFIED	UL

Body of the Final Report

CONTENT

1.Tasks of the Contract*.*

Fundamental investigations of physico-chemical mechanisms of combustion of new modern mixtures of HNIW (2,4,6,8,10,12-hexanitrohexaazaisowurtzitane) with new polymeric energetic binders, with burn-rate modifier, and mixtures of HMX with the same binders and the modifier, must be performed by study of burning wave structures and by obtaining burning rates and main burning wave parameters, first of all - burning surface temperatures. Processing of experimental data must allow leading stages and macrokinetics of gasification of solid phase in combustion waves to be established. Features of the combustion mechanisms of the mixtures under stable conditions must be formulated. Elaboration of closed system of predicting methods for pulsating burning rates, which are typical ones for rocket motors, must be performed at the second stage of the work. The system includes obtaining following special characteristics: erosive burning rates of the mixtures, estimations of pressure driven (coupled) burn-rate response functions on pressure pulsations, and estimations of hot gas velocity driven burn-rate response functions on gas velocity pulsations. The obtained corps of special characteristics must describe burning rate behavior of the mixtures inside rocket motors. The suggested approach must be based on unique methods for both stages.

Report must contain experimental results, results of processing of the experimentally obtained data, discussions, conclusions about combustion mechanisms of the studied mixtures under stable and pulsating external conditions, and recommendations.

Information about experimental techniques and arrangements must be suggested.

7. Objects of Investigations.

The following mixtures were investigated:

1) HNIW/(BAMO-THF), ratio 80:20, sum formula $O_{23,667}H_{23,737}N_{26,626}C_{18,690}$; sample density ρ = 1.65 g/cm^3, T_{adiab}=2674^{o}C (at 10 MPa);

2) HNIW/(BAMO-AMMO)+modifier, ratio for oxid./binder/modif. is 77:20:3, sum formula $O_{23,537}H_{24,697}N_{26,428}C_{18,348}Pb_{0.0387}$; density ρ =1.57 g/cm^3. T_{adiab}=2648^{o}C (at 10 MPa);

3) HMX/(BAMO-THF), ratio 80:20, sum formula $O_{23,368}H_{34,393}N_{26,328}C_{18,540}$; density ρ =1.69 g/cm^3. T_{adiab}=2171^{o}C (at 10 MPa);

4) HMX/(BAMO- AMMO)+modifier, ratio for oxid./binder/modif. is 77:20:3, sum formula $O_{232479}H_{34,953}N_{26,141}C_{18,205}Pb_{0.0387}$; density ρ =1.68g/cm^3. T_{adiab}=2164^{o}C (at 10 MPa);

Characteristics of ingredients were as follows: HNIW (CL-20) is a polycyclic caged nitramine, which have chemical nomination 2,4,6,8,10,12-hexanitrohexaaza-isowurtzitane; it is a powder with crystal particles of density ρ=2,01 g/cm^3; the particles have not regular shape and sizes from 1 up to 200 μm for mixture 1, and from 1 to 300 μm for mixture 2 (average mass sizes of the particles is 45 μm). HMX particles have sizes less than 315 μm. Energetic binder (BAMO-AMMO) is a copolymer of two thermoplastic elastomers - poly bis 3,3-azidomethyloxetane (BAMO) and poly 3-azidomethyl-3-methyloxetane (AMMO), in proportion 50:50. Energetic binder (BAMO –THF) is copolymer BAMO with tetrahydrofurane THF, in proportion 50:50. Stearate of Pb of chemical formula $(C_{17}H_{35}CO_2)_2Pb$ was used as a burn-rate modifier (or –as a promoter); addition of the modifier is 3% by mass. It is a powder with crystal particle sizes of 2-3 μm.

3. Experimental Techniques and Arrangements.

Cylindrical samples of the mixtures (8 mm in diameter and 3 cm in length) were burned in window bomb (volume 2000 cm^3) of constant pressure in atmosphere of gas nitrogen at pressures 0.5-10 MPa. The samples with 2-3 tungsten-rhenium microthermocouples imbedded inside, were placed into small thermostat inside the window bomb. One of copper-constantane thermocouple showed temperature of the thermostat. The inner volume of thermostat with sample was cooled by liquid nitrogen for obtaining negative sample temperature (-100^{o}C), or heated by electrically heated wire – for obtaining elevated positive temperature (+100^{o}C). The samples had been ignited by heated wire. Burning rates were measured by determination of time delay between the microthermocouple signals, by microfilming sample combustion and by determination of time of pressure increase during the sample combustion. Pressure in the bomb was measured by pressure detectors. Accuracy of pressure measurements is ±0.04 MPa. Temperature profiles of the combustion waves were measured by microthermocouple methods. Ribbon U-shaped thermocouples made of alloys (W+5%Re)/(W+20%Re) of 2-7 μm thick were imbedded into propellant samples. Thermocouple signals were recorded by amplifier and oscillograph.

Burning surface temperatures were measured by thermocouples that are being pressed to the surface during sample combustion and by establishing locations of slope breaks on measured temperature profiles. There is a theory of microthermocouple measurements of temperature profiles and burning surface temperature. There are experimental substantiations of burning surface temperature measurements by determination of temperature of the break. All requirements of the theory meet in these investigation and because of that all systematic errors were minimized. Instrument errors in microthermocouple measurements comprise about 1%.

Different types of metal wires for thermocouples were used (We,Re, and Pt,Rh) to test the catalytic effect on the thermocouples. This catalytic effect was not observed.

4. Results of Measurements at Pressure and Sample Temperature Variations.

The investigated mixtures burned at different pressures and sample temperature, as a rule, relatively steady, without regular periodically pulsations of burning rate.

4.1. Carbon residue. The studied mixtures 1, 2 have decreased carbon residue on the burning surface, in comparison with the previously investigated HNIW–based mixtures. Mixture 2 has

only slight soot formation on the burning surface at low pressures. Possibly, the very low carbon residue formation in combustion waves of this mixture is an action of burn-rate modifier, stearate of Pb. More significant carbon residue has mixture 1. A carbon lattice is created in combustion waves of this mixture at low pressures (0.5-1 MPa). This latter has a very low density and because of that gaseous combustion products blow easily through the lattice. Only separated blocks of the carbon lattice and flakes of soot are created during combustion of the mixture at 2 MPa. At 5 MPa only soot is observed. Carbon residue at 10 MPa isn't observed.

Experiments show that carbon residue formation on the burning surface of the studied mixtures practically doesn't depend on sample initial temperature. Carbon residue on the burning surface of mixtures on base of HMX (mixtures 3 and 4) isn't produced.

Results of experimental measurements of mass burning rates, burning surface temperatures, and other parameters of combustion waves of mixtures 1 - 4 show Tables 1 – 4. The Tables contain averages values of these parameters for every combustion regime. Figures 1 - 22 show averaged temperature profiles T(x) of mixtures 1 - 4, experimentally obtained at pressure and sample temperature variations.

4.2. Mass burning rates m. Tables 1 - 4 show that burning rates of mixtures on base of HNIW are higher significantly, than those of mixtures on base of HMX. Indeed, the burning rates of mixtures 1, 2 in the studied pressure interval change from 0.4-0.6 at 0.5 MPa to 3.0-3.9 g/cm^{2}s at 10 MPa (T_o=20^{o}C), but those of mixtures 3, 4 – from 0.25-0.35 (at 1 MPa) to – 1.15-1.65 g/cm^{2}s at 10 MPa (T_o=20^{o}C). The Tables also show that new active binder (BAMO-THF) in mixture with CL-20 have not very large burning rates – maximum m = 3.2 g/cm^{2}s at 10 MPa (T_o=20^{o}C). It is a moderate burning rate. Moderate burning rates have also mixture 2, having addition of Pb-stearate. Obviously, the burn-rate modifier significantly decreases m of mixture HNIW/(BAMO-AMMO), i.e. the mixture without the modifier (see below).

There are some peculiarities in combustion of the studied mixtures at low pressures. Mixtures 1 and 2 have stable combustion and temperature profiles T(x), beginning from 0.5 MPa at all investigated sample initial temperatures (from -100 to +100^{o}C).

Mixtures 3 and 4 have stable combustion and normal temperature profiles T(x) at positive sample temperatures, beginning from 1 MPa (mixture 3 can burn also from 0.5 MPa at T_o=100^{o}C). However, at T_o= -100^{o}C the mixtures can burn only beginning from 2 MPa, possibly because of significant heat losses in the burning samples.

Standard deviation of m measurements is about ±5 %.

4.3. Burning surface temperatures T_s. Tables 1 and 2 show that burning surface temperatures T_s of mixtures 1 and 2 are significantly lower than surface temperatures of mixtures 3 and 4. Indeed the surface temperatures of mixture 1 comprise 262-340^{o}C (0.5-10 MPa), and of mixture 2 - 280-354^{o}C (T_o=20^{o}C), whereas surface temperatures of mixture 3 and 4 are equal to 375-488^{o}C and 392-505^{o}C (T_o=20^{o}C), correspondingly. Sample temperature variation doesn't change this difference.

Standard deviation of T_s measurements is about ±5 %.

4.4. Temperature profiles in the gas phase: temperature and geometrical characteristics. Temperature distributions T(x) along combustion waves of the investigated mixtures have relatively small temperature pulsations at low pressures. The pulsations are more significant only for mixture 1, possibly due to elevated carbon residue creation and carbon flakes tearing off from the burning surface. At p>2 MPa the temperature profiles are relatively smooth for all investigated mixtures. From five to ten numbers of temperature profiles T(x) were obtained by thermocouple method for each combustion regime at different p and T_o, and then averaged curves of T(x) were obtained. Figures 1 – 22 present the obtained T(x), and Tables 1 – 4 - burning wave parameters. The Tables and Figures show that all mixtures have in the gas phase a two-zone structure of the profiles at low pressures. This two-zone structure (low-temperature, or first zone, and flame zone) exists for mixtures without the burn-rate modifier (mixtures 1 and 3) up to about 2 MPa (T_o=20^{o}C). At p>2 MPa both zones merge into one zone of the gas phase.

Mixtures with the modifier (mixture 2 and 4) have a very short first zone even at 0.5-1 MPa and at p>0.5-1 MPa both zones merge into one zone (T_o=20^{o}C).

Values of mean temperature of the first zone, T_1, at T_o=20^{o}C, for mixture 1 are equal to 950-1100^{o}C, and for mixture 3 - 950-1000^{o}C. The dark zones for mixture 2 and 4 (with modifier) exist at T_o=20^{o}C only at minimal studied pressures (0.5 MPa for mixture 2 and 1 MPa for mixture 4) and values of T_s are close to 1000^{o}C.

Standard deviation of T_1 measurements is about ±10 %.

Distances L_1 between the burning surface and the beginning of the flame zone (L_1 is the length of the first flame) decrease when pressure increases. Values of L_1 at T_o=20^{o}C for mixture 1 are equal to 1- 0.5 mm (0.5-2 MPa), and for mixture 3 - to 2-1 mm (1-2 MPa). Mixtures 2 and 4 at T_o=20^{o}C have the dark zones only at minimal pressures of these mixtures. Values of L_1 here are very small and comprise 0.3-0.4 mm. Burn-rate modifier decreases significantly values of L_1. It can be seen from Tables 6, 7, which contain comparisons of burning wave parameters of the mixtures with and without the modifier at T_o=20^{o}C. Indeed, mixture HNIW/(BAMO-AMMO), without the modifier, has the first zone up to 5 MPa, whereas practically the same mixture with modifier (mixture 2) has the first zone only at 0.5 MPa. Similar phenomenon takes place for HMX-based mixture (mixture 4). It is interesting to note, that mixture with binder (BAMO-THF) on base of HNIW (mixture 1) has smaller length of the first flame, than similar mixture on base of HMX (mixture 3).

Sample temperature variation changes values T_1 and L_1. Tables 1 – 4 and Figures 1 – 22 show, that T_1 changes similar to T_o, i.e. T_1 increases and decreases as T_o. Values of L_1 also increase when T_o increases and decrease when T_o decreases. It implies that the first flame (possibly, in it's second part) of the studied mixtures is, probably, an induction zone.

Distances L between the burning surface and the flame (up to about 0.99 T_f values) also decrease when pressure increases. In fact, L is the length of the gas phase reaction zone. Values of L at T_o=20^{o}C for mixture 1 are equal to 4-1.2 mm (0.5-10 MPa), for mixture 2 - to 3-1.8 mm (0.5-10 MPa), for mixture 3 - to 3.5-1.0 mm (1-10 MPa), and for mixture 4 - to 3-1 mm (1-10 MPa). It can be seen, that values of L for the studied mixtures are very close to each other.

Standard deviations of L_1 and L measurements are close to each other and comprise ±(10-20)%.

Flame temperatures T_f increase with pressure up to 3-5 MPa and then T_f reach maximal value for every mixture, which was close to thermodynamic calculated $T_{f.}$ for corresponding mixture. It can be seen, that values of T_f of HNIW-based mixtures are much higher than those of HMX-based mixtures.

Standard deviation of T_f measurements is about ±5 %.

5. Experimental Data Processing.

The processing of the obtained temperature profiles allows a set of burning wave parameters to be determined. Tables 1 - 4 present the dependencies of the parameters on pressure and initial sample temperature. Table 5 shows estimated due to gas product content the dependencies of coefficients of heat conduction λ_g and specific heat c_p of the gas phase on temperature.

5.1. Coefficients of heat diffusivity and heat conduction in solid heat layer.

Coefficients of solid heat diffusivity were obtained by formula $\chi = l \cdot r_b$, where l is thickness of heat layer of the condensed phase (see next section). Tables 1 - 4 show that values of χ increase when pressure increases. Estimations show that values of χ increase with pressure from $(1.2\text{-}2.6)\cdot 10^{-3}$ cm^2/s at 1 MPa up to $(2.1\text{-}5.5)\cdot 10^{-3}$ cm^2/s at 10 MPa (T_o=20^{o}C). These values are typical ones for χ of solid heat layer of many propellant mixtures.

The coefficients of solid heat conduction were obtained by formula $\lambda_s = \chi \cdot c \cdot \rho$. It was assumed that solid specific heat is equal to c=0.35 cal/g·K for mixtures 1 and 2 and c=0.4 cal/g·K for mixtures 3, 4. Estimations show, that λ_s increases with pressure. Values of λ_s comprise (8-

14)·10^{-4} cal/cm·s·K at 1 MPa and (14-29)·10^{-4} cal/cm·s·K at 10 MPa (T_o=20°C). These values are also typical ones for λ_s of solid heat layer of many propellant mixtures.

5.2. Characteristic sizes in the solid and gas phases.

Characteristic thickness *l* and l_m in solid, presented on Tables 1 - 4, were obtained by temperature distributions in the condensed phase. Experimentally obtained thickness of heat layer in solid *l* is a distance between the burning surface with temperature T_s and a section in solid with temperature $T^*=(T_s-T_o)/e + T_o$; (e is the base of ln). Thickness of l_m of the partly melt layer (with melt oxidizer) in the condensed phase is a distance between the burning surface and a section with oxidizer melt temperature T_m. It was assumed that the melt temperature for CL-20 is equal to T_m=190°C and for HMX - T_m=280°C. Tables show that thickness of *l* and l_m decrease when pressure increases. Values of l_m are always less than values of *l*. Values of *l* comprise 90-20 μm and l_m – 50-12 μm.

Conductive sizes ϑ of the gas phase were obtained by formula: $\vartheta=\lambda_g/mc_p$; where λ_g is coefficient of heat conduction in gas and c_p is coefficient of specific heat of the gas phase (see Table 5). Values of λ_g, which were used for ϑ calculations, were taken at temperatures T_1 for two-zone structures and at $T_f/2$ for one-zone structures. Tables 1 - 4 show that values of ϑ quickly decrease when pressure increases. Values of ϑ comprise 13-29 μm at 0.5-1 MPa and 2.5-5 μm at 10 MPa. It can be seen that always the following inequalities take place: $\vartheta<<L_1$ and $\vartheta<<L$.

Relative thickness of the gas-phase reaction layer Ω were estimated by formula $\Omega=L_1/\vartheta$ for two-zone structures, or by formula $\Omega=L/\vartheta$ for one-zone structures. It can be seen that inequality of $\Omega>>1$ always takes place. It implies that a wide reaction zone in the gas phase is observed for all combustion regimes of mixtures 1 – 4, at pressure and sample temperature variations.

5.3. Heat manifestations: heat release in solid and heat feedback from gas into solid.

The temperature profiles and burning surface temperatures were used for obtaining heat parameters of the burning waves. Heat flux from gas to solid q·m by heat conduction was estimated by the following formula:

$$q\cdot m=-\lambda_g(T)\cdot(dT/dx)_o; \qquad (5.1)$$

Here: $(dT/dx)_o=\varphi_o$ is the temperature gradient in gas close to the burning surface. Values of φ_o were determined by slopes of the temperature distributions T(x) in gas close to the surface.
Heat feedback q from gas into solid by heat conduction was estimated by the following formula:

$$q=-\lambda_g(T)\cdot\varphi_o/m; \qquad (5.2)$$

Values of λ_g were taken at temperatures $T=T_s+100^oC$.
Formula for heat release Q in reaction layer of the condensed phase (or on the burning surface) have the following forms:

for mixtures 1, 2 $$Q=c\cdot(T_s-T_o)-q-q_r; \qquad (5.3)$$

and

for mixtures 3, 4 $$Q=c\cdot(T_s-T_o)-q-q_r+q_m; \qquad (5.4)$$

where q_m is the heat of HMX melting in mixtures 3, 4; heat of HNIW's melting are not known and because of that formula for mixtures 1, 2 don't have member of q_m. Heat of HMX's melting is equal to 24 cal/g (per gram of HMX) and because of that q_m=19.2 cal/g for mixture 3, and q_m=18.5 cal/g for mixture 4. Radiant heat feedback q_r from flame into solid was estimated for all mixtures by using of content of combustion products and real flame thickness of the burning samples in the bomb of constant pressure. The heat radiations of CO_2, H_2O, H_2, etc were taken into considerations. It was assumed that coefficient of heat radiation absorption of the burning surface was equal to 0.5. Tables 1 - 4 show the obtained heat parameters.

It can be seen from Tables 1 - 4 that all investigated mixtures have significant positive heat release in solid Q. Parameter Q comprise at pressures 0.5-10 MPa the following values (T_o=20^{o}C): 64-95 cal/g for mixture 1, and 75-102 cal/g for mixture 2. This parameter for mixtures 3 and 4 at pressures 1-10 MPa has values 139-182 cal/g and 143-196 cal/g, correspondingly (T_o=20^{o}C). Parameter Q increases always with pressure. It can be seen that, as a rule, the values of Q for HMX-based mixtures significantly higher than those for HNIW-based mixtures.

Temperature gradient φ_o in gas close to burning surface has significant values {(3-20)·10^4, ^{o}/cm} and always increases with pressure. On the contrary, heat feedback q from gas into solid always decreases when pressure increases. Values of q are significantly smaller than values of Q, especially at elevated pressures. Indeed, Tables 1 - 4 show that q comprises in the studied pressure intervals the following values (at T_o=20^{o}C): 16-8 cal/g for mixture 1, 13-8 cal/g for mixture 2, 22-20 cal/g for mixture 3, and 25-13 cal/g for mixture 4. The values of q_r are small always and comprise 3-10 cal/g for HNIW-based mixtures and 0.3-5 cal/g for HMX-based mixtures. It can be seen, that total heat feedback $q+q_r$ from gas to solid surface are always less than heat release in solid, i.e. inequality $Q > q+q_r$ always takes place.

Sample temperature variations change values of φ_o, Q and q. As a rule, values of φ_o, q and Q increase when T_o decreases.

Tables 1 - 4 show that values of heat release rate F_o in gas near the burning surface (see n. 5.4) quickly increase with pressure. Values F_o comprise at To=20^{o}C (8.3-223)·10^3 cal/cm^{3}s - for mixture 1, (15.7-318)·10^3 cal/cm^{3}s- for mixture 2, (4-57)·10^3 cal/cm^{3}s - for mixture 3, and (7.5-83.5)·10^3 cal/cm^{3}s for mixture 4.

It can be seen, that HNIW-based mixtures have, as a rule, more intensive chemical reactions in gas near the burning surface, than mixtures on base of HMX.

Sample temperature variations insignificantly change values of F_o.

5.4. Distributions of the heat release rate in the gas phase.

The distributions of the heat release rate along the gas phase of the combustion wave can be obtained by the temperature profiles and by using equation of heat conduction for stable propagating combustion waves (coordinate x of the equation is connected with the burning surface). The equation has the following form:

$$d/dx(\lambda_g dT/dx)+mc_p(dT/dx)+F(x)=0; \qquad (5.6)$$

The term of F(x) in the equation was calculated for every regime of combustion by corresponding averaged temperature profiles T(x) in the gas phase, due to a special procedure of calculations of the first and the second terms of the equation. The procedure includes the technique of analytical fit of the profiles, and corresponding differentiations of the obtained analytical expressions with respect to x. The obtained distributions of F(x) at To=20^{o}C are presented in Tables 8-11 with the used averaged profiles T(x) (1 kcal/cm^{3}s =10^3 cal/cm^{3}s). It can be seen, that maximal heat release rate in the gas phase is observed always on the burning surface and that functions of F(x) quickly decrease with x increasing. Two-zone structures have additional zone of the heat release rate with a maximum in the middle of the first flame zone, and with a smooth curves before and after the maximum.

6. Discussions: Combustion Mechanisms at Stable Pressure.

6.1. Burning rate control regions.

The results of measurements of parameters $q+q_r$ and Q and the investigations of the gas phase zone behavior show that burning rate of the mixtures are caused by the heat release in solid (or on solid surface) and, in a smaller degree, by the heat feedback from the gas layer which is close to the burning surface. It was mentioned above also that the values of $q+q_r$ decreases when the burning rate increases. These facts show that heat release in solid (or on solid

surface) is a main factor of creating of the burning rate of the mixtures. Heat feedback from gas to solid is only small additional factor of the burning rate creating and influence of this factor on values of m decreases when pressure increases (at pressures $p \leq 10$ MPa). Then, the obtained data, presented in Tables 1 - 4, allow an important conclusion to be made: the high temperature region of the burning waves cannot affect the burning rate. Indeed, the influence of the heat release in the gas phase on the burning rate can be estimated by the following formula obtained as a solution of the heat conduction equation (5.6):

$$m \cdot q = \int_0^\infty F(x) \cdot \exp(-x/\vartheta) \cdot dx; \qquad (6.1)$$

This formula shows that influence of heat release in gas on m decreases very quickly when $x > \vartheta$. Tables 1, 2 show that values ϑ are small and they are significantly smaller than gas zone sizes L and L_1: see large values of Ω for all combustion regimes. It implies that high temperature region of the burning waves cannot significantly affect the burning rate. Thus the obtained results show that the burning rate control regions in the combustion waves for all regimes of the mixtures combustion, under investigated conditions, are the regions of heat release in solid just under the burning surface (or immediately on the burning surface) and thin low-temperature gas layers close to the burning surface with thickness about $x \approx \vartheta$. High temperature gas regions cannot significantly influence the burning rate, in fact, because of a very large heat resistance of the gas phase of the mixtures (i.e. due to very small values of λ_g).

It is important to stress, that received above results about burning rate control region are valid for both type of mixtures, based on HMX and on CL-20.

It is important to note also, that the indicated results are valid also for the systems with the burn-rate modifier.

Sample temperature variation doesn't change this conclusion.

6.2. Macrokinetics of solid gasification.

The following equation connects burning rate of solid with burn-surface temperature and macrokinetic characteristics of solid gasification:

$$m^2 = \lambda_s \rho / Q^2 \cdot \Re T_s^2 / E \cdot k_o Q^* \cdot 1/N \cdot \exp(-E/\Re T_s); \qquad (6.2)$$

where $N = 1/\eta_s + (1-\eta_s)/\eta_s \cdot \ln(1-\eta_s) - (q/Q) \cdot [\ln(1-\eta_s)]/\eta_s$; $\eta_s = Q/Q^*$; Q^* is the maximum of the heat release in solid, E is activation energy of limiting stage of the gasification process, T_s in K. For studied combustion waves $N \cong 1$. The expression was obtained by solution of system of two equations for the steady propagated burning wave: the heat conduction equation for solid phase and the equation of diffusion of reagents. The burning wave propagates due to heat release in solid Q and heat feedback from gas to solid $q+q_r$. Function of the volumetric heat release rate W_s in solid reaction layer was assumed as follows:

$$W_s(\eta, T) = Q^* k_o \cdot \rho \cdot (1-\eta) \cdot \exp(-E/\Re T); \qquad (6.3)$$

Here η is the reaction completeness ($\eta = \eta_s$ on the burning surface), k_o is the pre-exponent multiplier. The member $\exp(-E/\Re T_s)$ in the equation above plays the most important role in this formula. Because of that the connection m and T_s can be presented by the following simplified expression:

$$m = A \cdot \exp(-E/2\Re T_s); \qquad (6.4)$$

This expression has been designated "gasification law".

The results of measurement, presented in Tables 1 and 2, allow the following gasification law for mixtures 1 and 2, i.e. for mixtures, based on HNIW, to be obtained:

$$m=1.8\cdot10^{6}\cdot\exp(-32800/2\Re T_s);\quad (m \text{ in } g/cm^2s,\ T_s \text{ in K}) \qquad (6.5)$$

Possibly, value E=32800 kcal/mole is an activation energy of the limiting stage of the process of oxidizer CL-20 gasification in the reaction layer of mixtures 1 and 2.

The results of measurement, presented in Tables 3 and 4, allow the following gasification laws for mixtures 3 and 4, i.e. for mixtures, based on HMX, to be obtained:

$$\begin{aligned} &m=1.1\cdot10^{4}\cdot\exp(-28000/2\Re T_s);\ (m \text{ in } g/cm^2s,\ T \text{ in K}); \\ &\qquad\qquad (\text{valid at } T_s<500^oC), \\ &m=1.33\cdot10^{7}\cdot\exp(-50000/2\Re T_s);\ (m \text{ in } g/cm^2s,\ T \text{ in K}); \qquad (6.6) \\ &\qquad\qquad (\text{valid at } T_s>500^oC), \end{aligned}$$

The obtained value of activation energy of the gasification process is very close to that of cyclic nitramines. Possibly, gasification of oxidizer HMX in the reaction layer of burning mixtures 3 and 4 is the limiting stage of the process of the mixtures gasification.

It is important to stress, that the obtained gasification laws (6.5), (6.6) are valid for the mixtures without and with the burn-rate modifier, and that the macrokinetics were obtained at pressure and sample temperature variations.

6.3. Actions of stearate of Pb as a modifier of combustion.

Tables 6 and 7 show influence of addition of $(C_{17}H_{35}CO_2)_2Pb$ (3% instead of oxidizer) on the studied mixtures at To=20°C. It can be seen, that, first of all, the addition acts quite different on CL-20 based and HMX based mixtures. Indeed, the stearate of Pb significantly decreases burning rates of ([BAMO-AMMO]/CL-20) – about two times, and slightly increases burning rates of ([BAMO-AMMO]/HMX) – about on 0.1 g/cm^2s. Such difference in the action indicates on significant difference in chemical mechanism of controlling reactions in solid reaction layers of these mixtures. On this difference indicates also different gasification laws of these mixtures, established in section 6.2. However, inside of each class of mixtures (based on CL-20 or on HMX) the addition doesn't change the gasification law and the position of burning rate control regions. The modifier decreases influence of type of active binder in HNIW-based mixtures.

The influence on mixture ([BAMO-AMMO]/CL-20). Table 6 shows that addition of $(C_{17}H_{35}CO_2)_2Pb$ decreases T_s and heat release in solid Q, and significantly decreases flame temperature T_f and heat release rate close the burning surface W_o. The burning rate significantly decreases in spite of increasing φ_o, q and q_r. Structure of combustion wave remains without qualitative change: wide reaction zone of chemical reactions with distributed heat release rate in the gas phase and two-zone structure at low pressures (only the addition decreases values of L_1 and restricts the pressures of two-zone structure existing).

The influence on mixture ([BAMO-AMMO]/HMX). Table 7 shows that addition of $(C_{17}H_{35}CO_2)_2Pb$ stops combustion at 0.5 MPa, slightly increases burning rate m, surface temperature T_s and heat release in solid Q. The addition decreases heat feedback q, q_r and heat release rate close the burning surface W_o. But especially significant decreasing takes place for flame temperature T_f . This decreasing at simultaneous increasing mass burning rate indicates once more, that region of maximal temperature in combustion wave doesn't play significant role in burning rate creation (see also section 6.1.). Structure of combustion wave remains without qualitative change: wide reaction zone of chemical reactions with the distributed heat release rate in the gas phase and two-zone structure at low pressures (even pressure area of two-zone existing remains the same).

Sample temperature variations don't change these results.

Thus, the studied burn rate modifier $(C_{17}H_{35}CO_2)_2Pb$ shows itself as an inhibitor in mixture ([BAMO-AMMO]/CL-20), and as a weak catalyst in mixture ([BAMO-AMMO]/HMX. Place of action of this modifier is a whole burning wave, however the most important place of

the action, which control burning rate, is the limiting reactions in solid reaction layer and gas phase reactions close to burning surface.

6.4. Criteria of stable combustion.

The following temperature sensitivities of burning rates and burning surface temperatures were found from data, presented on Tables 1 - 4:

$\beta=(\partial \ln m/\partial T_o)_{p\text{-const}}$, - temperature sensitivity of mass burning rate;

$\mathbf{r}=(\partial T_s/\partial T_o)_{p\text{-const}}$, - temperature sensitivity of burning surface temperature;

The obtained results for the investigated mixtures are shown on Table 12, where indicated also the sensitivities for mixtures (BAMO-AMMO)/HNIW and (BAMO-AMMO)/HMX without modifier. It can be seen, that HNIW-based mixture have very low temperature sensitivities of burning rate and surface temperature – in comparison with those of HMX-based mixtures.

Table 12 also contains parameter **k**, which was found by formula $\mathbf{k}=\beta\cdot(T_s-T_o)$. It is Zeldovich's criterion of stable combustion. Value **k** is using for determination of combustion stability, when surface temperature changes insignificantly at pressure and sample temperature variations. The criterion predicts stable combustion at $\mathbf{k} < 1$. Table 12 shows, that HNIW-based mixtures 1 and 2 have always $\mathbf{k}<1$. It implies, that these mixtures have stable combustion under studied conditions.

A significant changing of the surface temperature of mixtures 3 and 4 takes place (see Tables 3 and 4). In this case at $\mathbf{k} > 1$ (at $\mathbf{k} < 1$ Zel'dovich's and Novozhilov's criteria are identical) Novozilov's criterion **k***, have to be used. The criterion predicts stable combustion at $\mathbf{k^*} < 1$. The formula for the criterion is as follows:

$$\mathbf{k^*}=(\mathbf{k}-1)^2/(\mathbf{k}+1)\mathbf{r}\ ; \qquad (6.7)$$

Calculated values of criterion **k*** for mixtures 3 and 4 show also Table 12. It can be seen that the inequality $\mathbf{k^*} < 1$ takes place for mixtures 3 and 4 at all investigated pressures and sample temperatures. It implies, that mixture 3 and 4 also always have stable combustion under studied conditions. Comparison values **k*** for mixtures 2 and (*) shows, that addition of Pb-stearate to mixture (*) lead to elimination of unstable combustion of mixture (BAMO-AMMO)/HNIW at $T_o=-100^oC$.

The Second Stage: Imitation of Rocket Chamber Conditions.

New energetic fuels have increased sensitivities to specific conditions of rocket motors.

Three problems have to be solved for clarification of burning rates changing under conditions of rocket motors: 1) increasing of burning rate, when hot gaseous products of burning blow up burning surface (effect of erosive burning); 2) behavior of burning rate at ambient pressure pulsations; and 3) behavior of burning rate at gas velocity pulsations. This stage of work suggests characterizations, obtained by solving these three problems for the studied mixtures. In fact, the obtained data can be treated as additional passport data of the mixtures.

7. Erosive Burning of The Studied Mixtures.

7.1. Models of erosive burning.

Propellant burning surface is subjected to hot gas blowing up in rocket chamber practically always. High density charging of rocket motors and using of high energetic fuels, like the studied, renders this problem to a very serious one. Increasing of burning rate at blowing up of the burning surface can lead to catastrophic chamber pressure. Because of that, it is necessary to have a procedure for prediction of characteristics of erosive burning. During last years a very serious experimental and theoretical works were performed in this field. As a result, a semi-

empirical system of erosion phenomena predictions was created. This system has experimental validation and describes behavior of erosive combustion of wide class of propellants, including similar to the studied ones. The system of calculations is based on three sources: 1) fundamental dependences, obtained at investigations of burning wave structures (profiles of temperatures and heat release rates in the gas phase; dependencies of changing of burning surface temperatures and heat release in solid, when pressure and burning rate change; macrokinetics of gasification); 2) aerodynamics of boundary layer; and 3) dependences for parameters, which characterize the burning surface roughness.

The structure of burning wave at erosion is found by solving of heat conduction equation for turbulent boundary layer. Mechanisms of transport of turbulent tension τ and transversal heat flow q_t are realized in stable turbulent flow by "moles". Because of that the following formulas can be introduced: $\tau_t=\eta_t \cdot dW/dz$ and $q_t= - \lambda_t \cdot dT/dz$, where W is gas velocity, z is coordinate, normal to burning surface; η_t and λ_t are coefficients of turbulent dynamic viscosity and turbulent heat conduction, correspondingly. It is convenient to present dW/dz in form df/dz*, where dimensionless gas velocity f=W/W*; and dimensionless coordinate z*=z/*l**; here dynamic velocity $W^*= (\tau_t/\rho)^{0.5}$; and $l^*= \upsilon/W^*$, where υ is kinematic viscosity of turbulent flow kernel. So, coefficient of turbulent heat conduction can be presented in the following form:

$$\lambda_t=\lambda/(df/dz^*); \qquad (7.1)$$

Function $\varphi`(z^*)= df/dz^*$, is universal one for all kind of turbulent flow kernels.

Formula (7.1) shows that influence of turbulence emerge in heat conduction only. So, turbulence of flow, blowing up the burning surface, can be taken in consideration by including into heat conduction equation the coefficient λ_t, presented by (7.1).

Real macrokinetics of combustion in the gas phase of combustion waves are introduced into the equation by F(z), obtained early (see n.5.4; here coordinate x replaced by coordinate z, adopted in this section, but coordinate x directed along vector of W). It can be seen, that here an assumption is made for the gas phase: chemistry and aerodynamics are independent. Large experience shows that this assumption is valid. Reason of this validity can be explained, possible, by the fact, that maximum of functions F(z) lies near surface, where intensity of turbulence is relatively small (namely vicinity of burning surface determines the burning rate - see n. 6.1).

Thus, the erosive burning rate can be obtained by solution of the following equation:

$$\partial / \partial z \ [\lambda_t(z) \ \partial T / \partial z \ ] - mc \cdot \partial T / \partial z + F(T, p) =0= c\rho(\partial T / \partial \tau); \qquad (7.2)$$

Where τ is current time (explanations – see below).

Functions F(T, p) were taken for calculations from Tables 8-11 (when calculation were performed for mixtures 1-4).

Bounder conditions: z=0; $T=T_s$; $\lambda(\partial T / \partial z)=[c_s(T_s-T_o) - Q_e(m, p)] \cdot m$;

$$z=D>> \lambda_t/cm; \quad T=T_f; \ (\partial T / \partial z)=0;$$

Initial condition: $T_s=T_{so}$; where T_{so} is surface temperature without erosion (see n.4.3).

Macrokinetics of solid phase gasification, presented by equations (6.6), (6.6), were introduced into program of erosive burning rate calculations. It is naturally, because connection between mass burning rate and surface temperature doesn't depend on reason of burning rate increasing.

Indicated in (7.2) function Q_e (heat release in solid at erosive burning) plays important role in erosive combustion. Values of Q_e was found by a special processing of obtained in n.5.3 values of heat release in solid Q. Experience showed, that values of Q can be used for obtaining

Q_e. For this purpose values of Q have to be presented as function on parameter $p/\sqrt{m}$; where *m* is erosive burning rate. In other words, $Q_e(m, p)=Q(p/\sqrt{m})$. These functions are presented below, in Eqs. (7.3).

Describing of aerodynamics of turbulent boundary layer was performed by two different models of hot gas flow, depending on character of burning surface. It is well known, that at stable erosion the burning surface is rough. This roughness is created by system of Tailor-Gertler's vortexes, and looks as systems of caverns and knobs. In this section we will obtain burning rates for two cases: for smooth surface and for rough surface. Results of calculations for smooth surface will be used only below, in n. 8.

Three-layer model of turbulent boundary layer is used in calculations for smooth burning surface. The main expressions of the model are as follows:

coefficient of friction $\xi=\xi(Re)$, where $Re=W\rho d/\eta$; $\xi=0.0032+0.221/Re^{0.237}$; $f=W(z^*)/W^*$; $W^*=W\cdot\sqrt{\xi/8}$; $z^*=z/l^*=z\cdot k_p$; where coefficient of turbulence $k_p=\frac{W\rho}{\eta}\cdot\sqrt{\xi/8}$;

Here W-mean value of flow velocity, $\rho=p/f_o$; $f_o=RT_f/\mu$; dynamic viscosity was found by formula; $\eta=3.945\cdot10^{-4}[0.714+0.358\cdot(T_f/1000)^2-0.0714\cdot(T_f/1000)^3]$; g/cm.s;

Functions f and df/dz* have the following forms:

if $z^*\le5$, then $f=z^*$; $df/dz^*=1$;

if $5<z^*\le30$, then $f=5+5\ln(z^*/5)$; $df/dz^*=5/z^*$;

if $z^*>30$, then $f=5.5+2.5\ln(z^*)$; $df/dz^*=2.5/z^*$;

Two-layer model of turbulent boundary layer is used for rough burning surface. The main expressions of the model are as follows:

coefficient of friction for rough surface $\xi_{rh}=\xi_{rh}(h_s)$, where $h_s=0.005$ cm for system of high burning rates and $h_s=0.004$ cm – for low burning rates. The values of h_s correspond to $Re_s=h_sk_p\ge60$ already at $W\ge100$ m/s. $\xi_{rh}=0.25/(\lg h_s/3.7d)^2$; where d-diameter of canal.

Functions f and df/dz* have the following forms:

if $z^*\le8.48$, then $f=z^*$; $df/dz^*=1$;

if $z^*>8.48$, then $f=8.48+2.5\ln(z^*)$; $df/dz^*=2.5/z^*$;

The following expressions were obtained and used in calculations for values of Q_e ($T_o=20^oC$):

$$\begin{aligned}
&\text{mixture 1;}\quad Q_e=100-54.6\cdot\exp[-0.0417\cdot(p/\sqrt{m})];\\
&\text{mixture 2;}\quad Q_e=115-47.94\cdot\exp[-0.0244\cdot(p/\sqrt{m})];\\
&\text{mixture 3;}\quad Q_e=190-81.45\cdot\exp[-0.0260\cdot(p/\sqrt{m})];\\
&\text{mixture 4;}\quad Q_e=210-109.95\cdot\exp[-0.0264\cdot(p/\sqrt{m})];
\end{aligned}\qquad (7.3)$$

Here Q_e in cal/g, *p* in atm, and *m* in g/cm^2s.

Temperatures of gas, which blow up the burning surface, were temperatures of flames of the studied mixtures.

Equation (7.2) was solved by a special program. It was combination of methods of "running" and "profile establishing". In the beginning of calculations the initial temperature profile and heat release rate were given for every regime. Calculations were performed up to establishing of stable temperature profiles, when $(\partial T/\partial\tau)=0$.

7.2. Results of erosive burning rate estimations of the studied mixtures.

Presented in the previous section models allows us to receive erosive burning rates of the studied mixtures, temperature profiles and surface temperature at erosive burning and distributions of heat release rate in the gas phase of combustion waves under condition of blowing up of the

burning surface. It is convenient to present effect of erosion on burning rate in form of erosive coefficient $\varepsilon=m/m_o$, where m is erosive burning and m_o is burning rate without blowing up of the surface. So, the main parameters of Tables 1-12 have to have in this section subscription $_o$.
Table 13 shows results of calculations by two-layer model. Coefficient of erosion ε, erosion burning rates m and burning surface temperatures T_s at erosion, are shown in Table 13 as functions of gas velocity W (base velocities are 100, 300, 600, and 800 m/s) and pressure (base pressures are 1, 5, and 10 MPa). All parameters were received here for point on the burning surface, which is on distance 100 mm from leading edge of propellant charge, and for $T_o=20^oC$. The stable erosive action is considered here, i.e. for rough surface. It is necessary to note, that dependence of the parameters, involved in the description, on the distance from leading edge of propellant charge is relative week. It can be seen from Table 13, that ε and m increase when pressure and W increase. Surface temperature T_s also increases with p and W. Physical reason of ε and m increasing is increased heat flux from gas into solid because of turbulence in the gas, i.e. due to turbulent heat conduction.
Analysis shows that CL-based mixtures have relatively small increasing of ε under studied conditions. Indeed, for mixture 1 values of ε increase at 1-10 MPa from 1.02-1.09 at W=100 m/s up to 1.63-2.54 at 800 m/s. Mixture 2 have values of ε increased in the pressure interval from 1.00-1.06 at W=100 m/s up to 1.44-2.12 at 800 m/s. However, HMX-based mixtures have very large response on hot gas blowing up of the burning surface. Indeed, for mixture 3 values of ε increase at 1-10 MPa from 1.91-2.11 at W=100 m/s up to 4.08-5.84 at 800 m/s. Mixture 4 have values of ε increased in this pressure interval from 1.67-2.17 at W=100 m/s up to 3.07-4.37 at 800 m/s. This effect is the main result of investigation of the problem: **mixtures with small initial burning rates have larger erosion, than mixtures, having high initial burning rates.**

7.3. Influence of Pb-stearate on erosive burning.

Table 13 contains results of calculations of erosion effects for mixtures (*) and (**) without burn rate modifier, Pb-stearate. It allows us to check influence of the modifier on erosive burning. In n. 4.3 was established, that burn rate modifier $(C_{17}H_{35}CO_2)_2Pb$ shows itself as an inhibitor in mixture ([BAMO-AMMO]/CL-20), and as a weak catalyst in mixture ([BAMO-AMMO]/HMX. Table 13 shows, that in line with this conclusion about action on burning rate,
the modifier increases ε of CL-based mixture and slightly decreases ε of HMX-base mixture.

So, we can repeat here, that effect of erosion more significant for mixtures with decreased initial burning rates, than for mixtures with increased burning rates.

7.4. "Sequence of preferences" for erosive burning.

From point of view of danger of large erosive coefficient, "sequence of preferences" for the studied mixtures has the following form (in the beginning - more preferable mixtures, having smallest erosion coefficient):

[(BAMO-AMMO)/HNIW, 20:80]>[(BAMO-AMMO)/HNIW+modif.]>
[(BAMO-THF)/HNIW, 20:80]>[(BAMO-AMMO)/HMX+modif.]> } (7.4)
[(BAMO-AMMO)/HMX, 20:80]>[(BAMO-THF)/HMX, 20:80];

8. Pressure Coupled Burn-Rate Response Functions of The Studied Mixtures.

Behavior of burning rate at ambient pressure pulsations is the second problem, which is necessary to clarify. This behavior can be described by the corresponding response functions. Pressure coupled response function can be obtained by differential coefficients (sensitivities) of burning rate and surface temperature. This obtaining is presented in the next paragraph.

8.1. Sensitivities of burning rates and surface temperatures to pressure and initial sample temperature.

The following pressure and temperature sensitivities for burning rates and burning surface temperatures were found from data presented on Tables 1-4:

$\beta=(\partial \ln m/\partial T_o)_{p\text{-const}}$, - temperature sensitivity of mass burning rate;

$\mathbf{r}=(\partial T_s/\partial T_o)_{p\text{-const}}$, - temperature sensitivity of burning surface temperature;

$\nu=(\partial \ln m/\partial \ln p)_{To\text{-const}}$, - pressure sensitivity of mass burning rate;

$\mu=(T_s-T_o)^{-1}\cdot(\partial T_s/\partial \ln p)_{To\text{-const}}$, - pressure sensitivity of burning surface temperature;

The obtained results for the investigated mixtures are shown on Tables 12 and 14.
Parameter **k** was found by formula $\mathbf{k}=\beta\cdot(T_s-T_o)$.

Sensitivity **ν.** It can be seen, that mixtures of binder (BAMO-THF) and oxidizers HNIW and HMX have close each other parameter **ν**. Indeed, mixture 1 has **ν**=0.56-0.68 at 0.5 MPa and **ν**=0.68 at 5-10MPa ($T_o=20^oC$), and mixture 3 has **ν**=0.65 at all pressures ($T_o=20^oC$). CL-based mixture with binder (AMMO-BAMO) and modifier has decreased **ν** in comparison with corresponding HMX-based mixture – for decreased pressures. Indeed, mixture 2 has **ν**=0.41-0.58 at 0.5-2 MPa, whereas mixture 4 has **ν**=0.56-0.66 (1-2 MPa). At 5-10 MPa both mixture have similar vales of **ν** (0.7-0.77 and 0.75, correspondingly). Modifier decreases values of **ν** for HNIW- and HMX-based mixtures at pressures 0.5-2 MPa. Indeed, in the case of HNIW-based systems, **ν**=0.5-0.8 for mixture (*) decreases up to **ν**=0.41-0.58 for mixture 2. In the case of HMX-based systems, **ν**=0.9-0.82 for mixture (**) decreases up to **ν**=0.56-0.66 for mixture 4. At increased pressures modifier practically doesn't change **ν**.

Sensitivity **β**. HNIW-based mixtures have more low values of **β**, than HMX-based mixtures. Indeed, mixture 1 has **β**=0.22-0.15 %/grad at 0.5-2 MPa and **β**=0.13 %/grad at 5-10 MPa, whereas mixture 3 has **β**=0.46-0.4 %/grad at 1-2 MPa and **β**=0.31-0.25 %/grad at 5-10 MPa. The same phenomenon takes place for mixtures with modifier: mixture 2 has **β**=0.185-0.1 %/grad at 0.5-2 MPa and **β**=0.09-0.085 %/grad at 5-10 MPa, whereas mixture 4 has **β**=0.335-0.3 %/grad at 1-2 MPa and **β**=0.27-0.16 %/grad at 5-10 MPa. Modifier Pb-stearate significantly decreases **β** of CL-based mixtures and increases **β** of HMX-based mixtures.

8.2. Burn-rate response functions on pressure pulsations.

The obtained results, which were received at constant, nonpulsating pressures, allow us to study burning rate behavior of the investigated mixtures under conditions of oscillatory pressure. It can be made due to obtained above sensitivities for m and T_s. This paragraph is devoted to this study.

We assume that external pressure changes by harmonic way and is equal to :

$$p=p_o+p`\cdot\cos\varpi t, \qquad (8.1)$$

here p_o is a constant mean pressure level and $p`$ is an oscillating pressure ($p` << p_o$), t is current time, and ϖ is cyclic frequency of oscillations in 1/s.

Then mass burning rate is equal to:

$$m=m_o+m`\cos(\varpi t+\psi)\ ; \qquad (8.2)$$

where m is current burning rate, m_o is stationary burning rate at pressure p_o , $m`$ is a pulsating burning rate ($m` << m$), and ψ is phase shift.

To study burning rate behavior under this condition, the following definition is used usually:

$$m`/m_o=U\cdot(p`/p_o); \qquad (8.3)$$

where U is response function of burning rate on pressure pulsations.

It is convenient to analyze burning rate response in complex form

The following expression was received by Novozhilov for burning rate response function to harmonic oscillatory pressure:

$$U = [\nu + (\nu \cdot r - \mu \cdot k) \cdot (z - 1)]/[1 + r \cdot (z - 1) - k \cdot (z - 1)/z]; \qquad (8.4)$$

Here $z=(1+\sqrt{1+4i\omega})/2$; and ω is dimensionless frequency, which is equal to the cyclic frequency ϖ, in 1/s, multiplied by the time of solid heat layer relaxation χ/r_b^2. Values of ν, μ, k and r here are based on the mean pressure p_o and because of that data from Table 14 can be used for estimations of complex functions of U. So, we can study the burning rate behavior of the investigated mixtures under conditions of pulsating pressure. The equation (8.4) is based on the supposition, that relaxation time of solid heat layer is much longer that those for reaction layer of solid and the leading part of the gas phase. Estimations show that for the investigated mixtures this supposition is valid: values of χ/r_b^2 are at least 10-20 times higher than other relaxation times. Because of that, all estimations of the response functions were made for dimensionless frequency interval ω=0-20.

Typical dimensionless amplitudes Re{U}of burning rate response functions and phase of the response, Im{U}, in radians, as dependencies on ω are shown on Figures 23-26 for mixture 1. Similar functions were obtained for other mixtures. Characteristics of the functions show Tables 15 and 16 (see below). It can be seen that the real part of U(ω) can reach values, which are much greater than its steady state value Re{U(0)}=ν. It is a consequence of high quality (in filter theory terminology) of our oscillatory systems, which are burning waves at pulsating pressures. The maximums of Re{U} are at a frequency, which are close to the natural (resonance) frequencies $\omega_n=\sqrt{k}$ /r. In this frequency area the denominator of equation (8.4) is less than unity. Because of that, any small perturbations in the pulsating system can significant influence the response function. It is natural, that function Im{U(ω)}, presenting the phase shift of the response function (see Figures 23-25), changes the sign at the resonance frequency.

Tables 15, 16 show results of calculations of characteristic points of Re{U} and Im{U} for the studied mixtures. Relative standard deviations of values $Re\{U\}_m$ obtaining are about $\pm$ (10 %).

The used denominations in Tables 15, 16 are as follows:

$Re\{U\}_m$ is maximum of Re{U($\omega=\omega_n$)} in interval ω=0-20; ω_n - dimensionless frequency, corresponding to this maximum (the resonance frequency); $Re\{U\}_{20}$ = Re{U(20)}; $Im\{U_{m+}\}$ - maximum of Im{U} in interval ω=0-ω_n, i.e. in positive region of values of ImU; ω_{im} - dimensionless frequency, corresponding to this maximum; $Im\{U_{m-}\}$ - minimum of ImU (if this minimum takes place) in negative region of ImU.

Figures 23-25 demonstrate typical functions Re{U(ω)}and ImU(ω)}, on example of the functions of mixture 1. Other mixtures have similar functions.

The most interesting parameters in Tables 15, 16 are $Re\{U\}_m$ and ϖ_n. The following conclusions can be made after observation of the obtained data:

1) CL-based mixtures, with binders (BAMO-THF) and (AMMO-BAMO)+modifier, have significantly more smal response $Re\{U\}_m$, than HMX-based mixtures; difference in $Re\{U\}_m$ can reach 2-3 times.
2) Modifier Pb-stearate, in binder (AMMO-BAMO), significantly decreases the response for CL-based mixture and increases the response for HMX-based mixture.
3) Without modifier the opposite situation occurs: oxidizer CL with binder (AMMO-BAMO) gives at 1-10 MPa higher response than HMX with the same binder.
4) Resonance frequencies ϖ_n quickly increase with pressure; values of ϖ_n weakly differs from each other for mixtures 1 and 2: from 0.2-0.7 kHz at 0.5 MPa till 8-9 kHz at 10 MPa.

Mixtures 3 and 4 have significantly lower ϖ_n: from 0.07-0.1 kHz at 0.5 MPa till

1.8-3.3 kHz at 10 MPa.

5) Modifier in binder (AMMO-BAMO) with CL decreases values of ϖ_n (at 2-10 MPa), but in the same binder with HMX the modifier increases ϖ_n.

8.3. "Sequence of preferences" for pulsating pressures.

Analysis of the obtained data for values of $Re\{U\}_m$ for the studied mixtures allows the following "sequence of preferences" for burning of these mixtures under conditions of pulsating pressure to be presented:

$$\left.\begin{array}{l}\text{[(AMMO-BAMO)/CL+Pb-stearate]> [(BAMO-THF)/CL, 20:80]>}\\ \text{>[(AMMO-BAMO)/HMX,20:80]>[(AMMO-BAMO)/CL, 20:80]>}\\ \text{>[(AMMO-BAMO)/HMX+Pb-stearate]>[(BAMO-THF)/HMX, 20:80];}\end{array}\right\} \quad (8.4)$$

In the beginning are the preferable mixtures, having smallest pressure-coupled burn-rate response near the resonance frequency (i.e. response $Re\{U\}_m$).

9. Velocity Coupled Burn-Rate Response Functions of The Studied Mixtures.

9.1. Statement of the problem.

The third phenomenon, which can affect the burning rate of propellant charge inside the rocket motor chamber, is pulsating hot gas velocity. This gas flows along the burning surface and has periodical small changing velocity. We assume that gas velocity changes by harmonic way and is equal to:

$$W=W_o+W`\cdot\cos\varpi t, \quad (9.1)$$

here W_o is a constant mean gas velocity level and W` is an oscillating velocity ($W` << W_o$), t is current time, and ϖ is cyclic frequency of oscillations in 1/s.

Then mass burning rate is equal to:

$$m=m_o+m`\cos(\varpi t+\psi)\ ; \quad (9.2)$$

where m is current burning rate, m_o is stationary burning rate, m` is a pulsating burning rate ($m` << m$), and ψ is phase shift.

Burning rate behavior under this condition can be described by a response function, which is introduced by the following definition:

$$m`/m_o=U_w\cdot(W`/W_o); \quad (9.3)$$

where U_w is response function of burning rate on gas velocity pulsations.

The physical reason of burning rate changing is periodical changing in blowing up of the burning surface by hot gas. This pulsating flowing creates a special effect and this effect we have to find. We will consider smooth burning surface. It is naturally to use in a way the steady effect of erosive burning. It can be obtained by three-layer model for smooth surface, described in n. 7. Figure 17 contains results of calculations of ε, received by the model for all studied mixtures.

The results, which were received under nonpulsating conditions, allow us to study burning rate behavior of the investigated mixtures under conditions of oscillatory gas velocity. It can be made due to sensitivities for m and T_s, which will be used together with erosive burning rate data.

It is convenient to analyze burning rate response in complex form, as in the previous case.

9.2. Solution of the problem.

The following expression was received for burning rate response function to harmonic oscillations of gas velocity:

$$U_w = [\nu_w + (\nu_w\cdot r_w - \mu_w\cdot k_w)\cdot(z - 1)]/[1 + r_w\cdot(z - 1) - k_w\cdot(z - 1)/z]; \quad (9.4)$$

Here $z=(1+\sqrt{1+4i\omega})/2$; and ω is dimensionless frequency, which is equal to the cyclic frequency ϖ, in 1/s, multiplied by the time of solid heat layer relaxation χ/r_b^2. The following formulas take place for parameters ν_w, k_w, r_w and μ_w**:**

$\nu_w=(\partial\varepsilon/\partial W_o)\cdot(W/\varepsilon)$;

$k_w=k\cdot\varepsilon$;

$r_w=\beta_w\cdot(\partial T_s/\partial \ln m)$; $\beta_w=\varepsilon\cdot\beta$;

$\mu_w=[\nu_w/(T_s-T_o)]\cdot(\partial T_s/\partial \ln m)$;

Values of k, β and ε, received before, show Tables 12, 13. The values are based on steady external conditions. Equation (9.4) is based on supposition: relaxation time of solid heat layer in combustion wave is much longer, than relaxation time of the gas phase of the wave. Estimations show that this supposition is valid.

The most important values of $(\partial\varepsilon/\partial W_o)$ can be obtained from dependences $\varepsilon=\varepsilon(W_o)$; and values of $(\partial T_s/\partial \ln m)$ can be obtained from macrokinetic laws (6.5), (6.6). However, dependency of U_w on ω has one specific feature. Namely, hot gas blowing of the burning surface can manifest itself in full scale only at ω=1, because it corresponds to maximal time of action. At more short time of action, i.e. at ω>1, coefficient of erosion ε_i have to be smaller. Because of that, it was assumed, that at ω>1 the values of ε_i (coefficient of erosion at ω>1) depend on ω by the following formula:

$$\varepsilon_i(\omega)=[(\varepsilon-1)/\omega]+1;$$

It can be seen, that $\varepsilon_i=\varepsilon$ at ω=1. Correspondingly, values of U_w at ω=1 have to be obtained by $(\partial\varepsilon/\partial W_o)$, and at ω>1 by $(\partial\varepsilon_i/\partial W_o)$. It implies, that for interval ω=0-1 values of U_w can be received by $(\partial\varepsilon/\partial W_o)$, but dependences $U_w(\omega)$ at ω>1 for every regime of combustion can be obtained only for integer values of ω (for instance, $U_w(\omega=2)$ has to be received by using $\partial\varepsilon_2/\partial W_o$, and so forth).

In calculations based values of W_o were taken as 300 and 600 m/s, and based pressures were 1, 5 and 10 MPa. Figures 26-31 shows obtained dependencies $\mathrm{Re}\{U_w(\omega, p, W_o)\}$ for the studied mixtures, on examples of the functions for W_o=300 m/s. Similar functions were receive for W_o=600 m/s. Dependencies for Im U_w are not interesting: as a rule, values of Im U_w are very small and practically always are positive (it implies delay in burn-rate response in comparison with velocity pulsations).

Table 18 demonstrates the main parameters of these functions. Nominations here are as follows: $\mathrm{Re}\{V_w\}_{max}$ is maximal value of real part of burning rate response function to oscillations of gas velocity, $\omega_{Re\ max}$ is dimensionless frequency for $\mathrm{Re}\{V_w\}_{max}$, ϖ is cyclic frequency in kHz for

$\mathrm{Re}\{V_w\}_{max}$, and $\omega_n=\sqrt{k_w}/r_w$ is normal (or, resonance) dimensionless frequency for this regime of combustion. It can be seen, that CL-based mixtures 1 and 2 have similar dependences $\mathrm{Re}\{V_w(\omega)\}$at all pressures and gas velocities, with small values of the maximum at ω=1 and decreased functions $\mathrm{Re}\{V_w(\omega)\}$ with ω increasing up to ω=5. Values of $\omega_{Re\ max}$ are equal to one for all combustion regimes of the mixtures. **Small values of $\mathrm{Re}\{V_w\}_{max}$ for mixtures 1, 2 signify, that burning rates of CL-based mixtures are highly tolerant to velocity pulsations of hot gas blowing up flow.**

The situation for HMX-based mixtures 3 and 4 is different: there are regimes of combustion and frequencies of velocity pulsations, at which $\mathrm{Re}\{V_w\}_{max}$ has large values. Indeed, it is equal to 8.3 for mixture 3 at 5 MPa, and 300m/s ($\omega_{Re\ max}$=4); and 1.63 for mixture 4 at 1 MPa, and 600 m/s ($\omega_{Re\ max}$=4). **It implies, that burning rates of HMX-based mixtures can be very sensitive to velocity pulsations of hot gas blowing up flow.**

The physical reason of the obtained conclusions is, possibly, the fact, that CL-based mixtures have values of dimensionless resonance frequencies ω_n, which are larger than region of ω=1-5. Indeed, ω_n is equal here to 7.4-11.5. However, for HMX-based mixtures values of ω_n are very close to values of $\omega_{Re\ max}$.

Addition of Pb-stearate to CL-based mixtures increases $Re\{V_w\}_{max}$ insignificantly. For HMX-based mixtures this addition increases $Re\{V_w\}_{max}$ more noticeably.

9.3. "Sequence of preferences" for pulsating hot gas flows.

Analysis of the obtained data for values of $Re\{V_w\}_{max}$ for every W_o allows the following "sequences of preferences" for burning of the mixtures under conditions of pulsating hot gas flow to be presented:

A. W_o=300 m/s.

[(AMMO-BAMO)/CL, 20:80]> [(BAMO-AMMO)/CL+Pb-stearate]>
>[(AMMO-BAMO)/HMX,20:80]>[(BAMO-THF/CL, 20:80]>
>[(AMMO-BAMO)/HMX+Pb-stearate]>[(BAMO-THF)/HMX, 20:80]; (9.5)

B. W_o=600 m/s.

[(AMMO-BAMO)/CL, 20:80]> [(BAMO-THF)/HMX, 20:80]>
>[(AMMO-BAMO)/CL+Pb-stearate]>[(BAMO-THF)/CL, 20:80]>
>[(AMMO-BAMO)/HMX, 20:80]>[(BAMO-AMMO)/HMX+Pb-stearate]; (9.6)

In the beginning are the preferable mixtures, having smallest velocity-coupled burn-rate response.

It can be seen, that the sequences are very close each other for both W_o, except position of mixture 3: at W_o=300 m/s the mixture has the end place, but at W_o=600 m/s it has even the second place. Possible, this result indicates on danger of gas velocity pulsations for mixture 3 at relatively small gas velocities, which are not far from threshold gas velocity (the threshold velocities of the studied mixtures are equal to ~ 50-150 m/s).

10. Comparison of "Sequences of Preferences".

It is interesting to compare the obtained "sequences of preferences", presented in (7.4), (8.4), (9.5) and (9.6). It is convenient to show these sequences in a following short form:

erosion burning - (*)>(2)>(1)>(4)>(**)>(3); (7.4)
pressure pulsating - (2)>1)>(**)>(*)>(4)>(3); (8.4)
gas velocity pulsating at W_o=300m/s - (*)>(2)>(**)>(1)>(4)>(3); (9.5)
gas velocity pulsating at W_o=600m/s - (*)>(3)>(2)>(1)>(**)>(4); (9.6)

The nominations of mixtures in brackets are the same as in Table 18.

It can be seen, that, in spite of differences in mixture positions for different phenomena, some common features can be observed. Indeed, the first places occupy mixtures **(*)** - (AMMO-BAMO)/CL, and **(2)** - (AMMO-BAMO)/CL+Pb-stear.; and the end places occupy most often mixture **(3)** - (BAMO-THF)/HMX. **Because of that it can be concluded, that CL-based mixtures (*) and (2) have minimal sensitivities to considered phenomena, and HMX-based mixture 3 have maximal sensitivities in the studied group of mixtures. It's obvious, that the minimal solid fuel sensitivity to the considered phenomena decreases danger of catastrophic pressures inside working rocket motors.**

Conclusions about Combustion Mechanisms of the Studied HNIW- and HMX-based Mixtures

Detailed characterizations of parameters of combustion waves of CL- and HMX-based mixtures were made by experimental measurements and by processing of experimental data at different stable pressures and sample initial temperatures.

Combustion mechanisms of mixtures ([BAMO-THF]/CL-20, 20:80) and ([BAMO-THF]/HMX, 20:80) at steady combustion.

Oxidizer CL-20 gives in mixture with (BAMO-THF) significantly higher flame temperature T_f (on 500^o!) and higher specific impulse (on 12 kg-force/kg), than oxidizer HMX.

This CL-based mixture has 2.5-2.8 times higher burning rates, than the corresponding HMX-based mixture.

Peculiarities of physical parameters of burning waves of CL-based mixture, in comparison with those of HMX-based mixtures, are as follows:

surface burning temperatures T_s is less (on about 100^o), than those of HMX-based mixtures;

heat feedback q is also less (at elevated pressures);

heat release in solid Q is about two times less, than that of HMX-based mixtures;

heat release rates in gas close to burning surface F_o are about three times more, than those of HMX-based mixtures.

distributions of the heat release rate along the gas phase of combustion waves

Different gasification laws were established for CL- and HMX-based mixtures:

$m=1.8\cdot10^6\cdot\exp(-32800/2\Re T_s)$; (m in g/cm^{2}s, T_s in K) – for CL-based mixtures, and

$m=1.1\cdot10^4\cdot\exp(-28000/2\Re T_s)$; (m in g/cm^{2}s, T in K) - for the HMX-based mixtures.

Both mixtures share the following common characteristic features of the investigated combustion waves:

burning rate control regions in the combustion waves are the regions of the heat release in solid and thin low-temperature gas layer close to the burning surface;

wide reaction zone of chemical reactions with distributed heat release rate in the gas phase; the obtained heat release rate distributions for all regimes of combustion have maximum of the rates close the surface and decreased character with coordinate increasing;

two-zone structure in the gas phase at low pressures.

Combustion mechanisms of mixtures ([BAMO-AMMO]/CL-20, 20:80) and ([BAMO-AMMO]/HMX, 20:80), without and with addition of $(C_{17}H_{35}CO_2)_2Pb$.

The addition acts quite different on CL-based and HMX-based mixtures: the addition significantly decreases burning rates of ([BAMO-AMMO]/CL-20) – about two times, and slightly increases burning rates of ([BAMO-AMMO]/HMX) – about on 0.1 g/cm^{2}s.

Such difference in the action indicates on significant difference in chemical mechanisms of controlling reactions in solid reaction layer of these mixtures, what is in consent with the indicated above difference in gasification laws.

Peculiarities of the modifier action on parameters of burning waves of CL-based mixture, in comparison with the action on HMX-based mixtures, are as follows:

surface burning temperature T_s of CL-based mixture slightly decreases, whereas for HMX based mixtures T_s increases;

heat feedback q of CL-based mixture increases, whereas for HMX-based mixtures q decreases;

heat release in solid Q of CL-based mixture decreases, whereas for HMX-based mixtures Q significantly increases;

heat release rate in gas close to burning surface F_o of both mixtures, as a rule, decreases.

Place of action of this modifier is a whole burning wave, but the most important place is the limiting reactions in solid reaction layer and gas phase reactions near the surface.

The modifier doesn't change the indicated above gasification laws and common characteristic features of combustion waves of the investigated mixtures.

Studied mixtures have steady combustion at used pressures and sample temperatures.

Sensitivities of burning rates to pressure and sample temperature.

CL- and HMX-based mixtures have not very far differed values of pressure sensitivities of burning rates for most regimes of combustion. Modifier decreases, as a rule, the sensitivities.

CL-based mixtures have more low values of temperature sensitivity of mass burning rate, than those of HMX-based mixtures. Modifier significantly decreases this sensitivity for CL-based mixtures and increases the sensitivity for HMX-based mixtures.

Conclusion On Imitation of Rocket Chamber Conditions.

1) Erosive burning characterizations of the investigated mixtures.

Special semi-empirical models were used for receiving characteristics of combustion waves transformed by erosive burning. The theory of turbulent boundary layer and obtained heat release rate distributions without blowing were used for the receiving. Erosive burning rates of the studied mixtures, temperature profiles, surface temperatures and distributions of heat release rate in gas at erosion were obtained for different gas velocities. **The main result of the investigation is as follows: mixtures with small initial burning rates (it is HMX-based mixtures) have larger erosion, than mixtures, having high initial burning rates (it is CL-based mixtures**).

The characterization of erosive burning gives in the work in quantitative and quality forms. Values of erosive burning rates were presented for different pressures and gas velocities, and "sequence of preferences" for the studied mixtures was given. From point of view of danger of large erosive burning rate increasing, the sequence has the following form (in the beginning - more preferable mixtures, having smallest erosion coefficient):

[(BAMO-AMMO)/HNIW, 20:80]>[(BAMO-AMMO)/HNIW+modif.]>
>[(BAMO-THF)/HNIW, 20:80]>[(BAMO-AMMO)/HMX+modif.]> (erosive burning)
>[(BAMO-AMMO)/HMX, 20:80]>[(BAMO-THF)/HMX, 20:80];

2) Burning rate response on pressure and gas velocity pulsations.

The study of burning rate behavior under conditions of oscillatory pressure was performed by response functions of burning rate on pressure pulsations. This function U has the following definition: $m`/m_o=U\cdot(p`/p_o)$; where parameters with $_o$ are constant and with` are pulsating ones. There is analytical solution for dependency U on pressure and temperature sensitivities for burning rates and burning surface temperatures, obtained before (see above) at stable combustion. This solution was used for obtaining the pressure-coupled burn-rate response functions U of the studied mixtures for different combustion regimes. The following conclusions were made after observation of the obtained data:

CL-based mixtures, with binders (BAMO-THF) and (AMMO-BAMO)+modifier, have significantly more small maximal real response amplitude $Re\{U\}_m$, than HMX-based mixtures; the difference in amplitude can reach 2-3 times.
Modifier Pb-stearate, in binder (AMMO-BAMO), significantly decreases the response for CL-based mixture and increases the response for HMX-based mixture.
Without modifier the opposite situation occurs: oxidizer CL with binder (AMMO-BAMO) gives at 1-10 MPa more high response, than HMX with the same binder.

Burning rate behavior under condition of gas velocity pulsations can be described by gas velocity coupled burn-rate response function U_w, which is introduced by the following definition: $m`/m_o=U_w\cdot(W`/W_o)$; where parameters with $_o$ are constant and with` are pulsating ones. The physical reason of burning rate changing is periodical changing in blowing up of the burning surface by hot gas. Analytical solution for dependency U_w on transformed pressure and temperature sensitivities for burning rates and burning surface temperatures, and also on erosive effect, were used. This solution was used for obtaining the velocity-coupled burn-rate response

functions U_w of all mixtures for different combustion regimes and gas velocities. The following conclusions were received:

Small values of maximal real response amplitude $Re\{V_w\}_{max}$ obtained for CL-based mixtures, signify that burning rates of the mixtures are highly tolerant to velocity pulsations of hot gas flow.

Increased values of $Re\{V_w\}_{max}$ obtained for HMX-based mixtures, implies that burning rates of the mixtures can be very sensitive to velocity pulsations of hot gas flow.

The characterization of sensitivity of burning rates to pressure and gas velocity pulsations have quantitative and quality forms. The work presents quantitative characteristics of maximal burn-rate response functions on pressure and gas velocity pulsations. The work also presents correlated analysis in a form of "sequences of preferences" for the studied mixtures. From point of view of danger of large burning rate increasing at pressure and gas velocity pulsations, the sequences have the following form (in the beginning - more preferable mixtures, having smallest burn-rate responses):

[(AMMO-BAMO)/CL+Pb-stearate]> [(BAMO-THF)/CL, 20:80]>
>[(AMMO-BAMO)/HMX,20:80]>[(AMMO-BAMO)/CL, 20:80]> (pressure-coupled pulsations)
>[(AMMO-BAMO)/HMX+Pb-stearate]>[(BAMO-THF)/HMX, 20:80];

Velocity 300 m/s.
[(AMMO-BAMO)/CL, 20:80]> [(BAMO-AMMO)/CL+Pb-stearate]>
>[(AMMO-BAMO)/HMX,20:80]>[(BAMO-THF/CL, 20:80]> (velocity-coupled pulsations)
>[(AMMO-BAMO)/HMX+Pb-stearate]>[(BAMO-THF)/HMX, 20:80];

Velocity 600 m/s.
[(AMMO-BAMO)/CL, 20:80]> [(BAMO-THF)/HMX, 20:80]>
>[(AMMO-BAMO)/CL+Pb-stearate]>[(BAMO-THF)/CL, 20:80]> (velocity-coupled pulsations)
>[(AMMO-BAMO)/HMX, 20:80]>[(BAMO-AMMO)/HMX+Pb-stearate];

Observations of the sequences show, that, in spite of differences in mixture positions for different phenomena, some common features can be seen. Indeed, the first places occupy mixtures (AMMO-BAMO)/CL, and (AMMO-BAMO)/CL+Pb-stearate; and the end place occupy most often mixture (BAMO-THF)/HMX. Because of that it can be concluded, that these CL-based mixtures have minimal sensitivities of burning rate to considered phenomena, and the HMX-based mixture have maximal these sensitivities in the studied group of mixtures. **Small sensitivity of solid fuel burning rate to the considered phenomena (pressure and velocity pulsations) implies decreased danger of catastrophic pressure appearing inside working rocket motors**.

RECOMMENDATIONS

It would be very useful from practical point of view to use the created system of experimental, semi-empirical and theoretical methods for investigations of combustion of the mixtures, having maximal energy (maximal specific impulse) in this class of rocket fuels.

TABLES of Final Report, N62558-03-M-0812

Table 1: Burning wave parameters of mixture 1 ([BAMO -THF]/CL-20, 20:80).

Parameters are presented at the following values of T_o: -100°C /20°C /100°C.

	p, MPa	0.5	1	2	5	8	10
1	m, g/cm^{2}s	0.4/0.42 /0.6	0.55/0.62 /0.8	0.9/1.0 /1.15	1.65/1.92 /2.14	2.2/2.55 /2.82	2.5/2.98 /3.25
2	T_s, °C	260/262 /275	272/276 /285	290/294 /300	315/320 /325	326/335 /338	332/340 /343
3	$\varphi_{o \cdot 10^{-4}}$, °/cm	2.7/4.0 /2.2	5.0/5.5 /4.5	7.0/7.0 /6.0	9.0/9.0 /8.3	10/11 /10	11/12.5 /11.5
4	q, cal/g	11.5/16 /6.0	16.4/24 /10	14.4/13 /10	9.0/9.0 /8.0	8.6/8.0 /7.0	8.4/8.0 /7.0
5	q_r, cal/g	5/5 /3	4.5/5 /3	5.6/5 /4	8.5/7 /7	11/9 /9	12/9 /10
6	Q, cal/g	110/64 /52	109/61 /102	117/78 /56	127/89 /64	130/92 /68	131/95 /68
7	l, μm	85/75 /70	65/56 /55	50/40 /45	35/28 /38	30/22 /33	26/20 /30
8	l_m, μm	30/35 /50	22/30 /40	18/26 /35	16/22 /32	14/18 /30	12/16 /30
9	T_1, °C	850/950 /1050	900/1000 /1100	-/1100 /1180	-/-/-	-/-/-	-/-/-
10	T_f, °C	2000/2400 /2480	2350/2500 /2580	2450/2550 /2630	2560/2675 /2770	2560/2675 /2770	2560/2675 /2770
11	L_1, mm	1.5/1.0 /1.8	0.5/0.8 /1.0	-/0.5 /0.7	-/-/-	-/-/-	-/-/-
12	L, mm	4.0/4.0 /4.2	2.5/3.0 /3.5	1.8/2.5 /2.8	1.5/2.0 /2.2	1.3/1.8 /2.0	1.2/1.2 /1.8
13	ϑ, μm	19.3/19.0 /14.5	14.5/13.0 /11.2	11.0/9.0 /8.0	6.0/4.7 /4.7	4.5/3.5 /3.5	4.0/3.1 /3.0
14	Ω	78/52 /124	34/61 /90	164/56 /88	250/426 /468	290/514 /570	300/387 /600
15	$F_{o \cdot 10^{-3}}$, cal/cm^{3}s (at T_o=20°C)	8.3	19.7	35.4	87.8	146	223

Table 2: Burning wave parameters of mixture 2
([BAMO -AMMO]/CL-20 +Stearate Pb, 20:77:3),

Parameters are presented at the following values of T_o: -100°C /20°C /100°C.

	p, MPa	0.5	1	2	5	8	10
1	m, g/cm^{2}s	0.56/0.68 /0.78	0.72/0.9 /0.98	1.1/1.3 /1.35	2.1/2.32 /2.5	2.95/3.28 /3.5	3.48/3.92 /4.2
2	T_s, °C	272/280 /284	282/290 /293	298/304 /306	323/328 /332	340/345 /348	348/354 /357
3	$\varphi_{o \cdot 10^{-4}}$, °/cm	6.0/5.0 /3.0	7.0/7.0 /5.0	9.0/9.0 /7.5	12.8/13.0 /12.0	14.5/15.0 /14.0	15.5/16.0 /15.0
4	q, cal/g	18.2/13 /7.0	17.5/14.0 /9.0	15.0/13.0 /10.0	11.3/11.0 /9.0	9.3/8.8 /8.0	8.7/8.0 /7.0
5	q_r, cal/g	3.6/3.0 /2.6	3.5/3.3 /2.6	4.5/3.8 /3.7	6.7/6.0 /5.6	8.0/7.2 /6.8	9.0/7.0 /7.5
6	Q, cal/g	108/75 /55	113/77 /56	120/83 /58	131/91 /67	137/98 /72	139/102 /75
7	*l*, μm	80/50 /60	65/45 /50	50/40 /45	35/30 /28	28/24 /20	25/22 /18
8	l_m, μm	25/30 /45	22/26 /35	18/22 /32	16/18 /25	14/17 /20	12/16 /18
9	T_1, °C	900/1000 /1050	-/- /1150	-/-/-	-/-/-	-/-/-	-/-/-
10	T_f, °C	2300/2300 /2420	2400/2400 /2520	2480/2500 /2600	2520/2630 /2740	2520/2630 /2740	2520/2630 /2740
11	L_1, mm	0.3//0.4 1.0	-/- /0.6	-/-/-	-/-/-	-/-/-	-/-/-
12	L, mm	2.5/3.0 /3.5	2.5/2.5 /3.0	2.8/3.0 /3.0	2.0/2.5 /3.0	1.5/2.0 /2.5	1.2/1.8/ /2.0
13	ϑ, μm	14.0/1.0 /11.3	13./11.0 /9.7	8.6/7.5 /7.2	4.6/4.3 /4.0	3.3/3.0 /2.8	2.8/2.5 /2.4
14	Ω	20/31/ 88	190/236 /62	325/400 /416	435/580 /750	450/667 /890	430/720 /830
15	$F_{o \cdot 10^{-3}}$, cal/cm^{3}s (at T_o=20°C)	15.7	29.5	55.3	147	245	318

Table 3: Burning wave parameters of mixture 3 ([BAMO -THF]/HMX, 20:80).

Parameters are presented at the following values of T_o: -100°C /20°C /100°C.

	p, MPa	0.5	1	2	5	8	10
1	m, g/cm^{2}s	-/- /0.3	0.18/0.26 /0.45	0.29/0.4 /0.63	0.56/0.73 /1.0	0.8/1.0 /1.3	0.93/1.16 /1.5
2	T_s, °C	-/- /385	353/375 /415	385/408 /443	447/456 /480	463/480 494	474/488 /500
3	$\varphi_{o} \cdot 10^{-4}$, °/cm	-/- /1.5	-/3.0 /2.0	5.0/4.0 /2.7	8.0/6.5 /5.0	10/9 /7.2	11.5/10 /8.3
4	q, cal/g	-/- /10	-/22 /8.9	34.5/20 /9.4	30/19.6 /11.5	27.5/20 /13	2702/19.8 /13
5	q_r, cal/g	-/- /0	-/0.4 /0.2	0.6/0.4 /0.3	2.8/2.1 /1.5	4.2/3.4 /2.6	6.2/5.0 /3.9
6	Q, cal/g	-/- /123	-/139 /136	178/154 /147	205/172 /158	213/180 /161	215/182 /162
7	l, μm	-/- /72	-/70 /56	90/60 /46	50/45 /36	40/35 /30	35/30 /27
8	l_m, μm	-/- /50	-/35 /40	25/25 /30	20/20 /22	18/18 /20	16/15 /18
9	T_1, °C	-/- /900	-/950 /1000	900/1000 /1050	-/-/-	-/-/-	-/-/-
10	T_f, °C	-/- /-	-/1900 /1950	1900/2000 /2100	2050/2170 /2270	2050/2170 /2270	2050/2170 /2270
11	L_1, mm	-/- />5	-/2.0 /2.2	0.5/1.0 /1.5	-/-/-	-/-/-	-/-/-
12	L, mm	-/- />5	-/3.5 /4.0	2.0/2.5 /3.5	1.5/2.0 /3.0	1.2/1.5 /2.5	1.0/1.0 /1.6
13	ϑ, μm	-/- /25	-/29 /17	25/20 /13	14/11 /8.6	9.7/8.0 /6.5	8.3/4.7 /5.7
14	Ω	-/- /-	-/69 /130	20/50 /115	107/182 /350	124/188 /385	120/212 /280
15	$F_{o} \cdot 10^{-3}$, cal/cm^{3}s (at T_o=20°C)	-	4.0	8.0	23.9	43.3	57

Table 4: Burning wave parameters of mixture 4 ([BAMO -AMMO]/HMX+Stearate Pb., 20:77:3).

Parameters are presented at the following values of T_o: -100°C /20°C /100°C.

	p, MPa	1	2	5	8	10
1	m, g/cm^{2}s	-/0.34 /0.46	0.4/0.5 /0.69	0.8/0.96 1.2	1.13/1.4 /1.62	1.34/1.63 /1.85
2	T_s, °C	-/392 /416	405/425 /450	463/477 /490	486/497 /505	495/505 /510
3	$\varphi_{o \cdot 10}^{-4}$, °/cm	-/4.5 /3.0	7.0/6.0 /5.0	10/8.0 /7.0	10/9.0 /8.0	11/9.5 /9.0
4	q, cal/g	-/24.5 /13.7	35/25.2 /16	24/18.5 /13.4	20/15 /11.4	19/13.3 /11.2
5	q_r, cal/g	-/0.32 /0.2	0.4/0.32 /0.2	2.0/1.6 1.3	3.0/2.5 /2.1	3.5/3.5 /3.5
6	Q, cal/g	-/143 /131	185/155 /142	216/181 /160	230/192 /167	235/196 /168
7	*l*, μm	-/70 /	40/6 /	30/40 /	24/35 /	22/30 /
8	l_m, μm	26/35 /	22/25 /	18/20 /	17/18 /	16/17 /
9	T_1, °C	-/1000 /1000	-/- /1100	-/-/-	-/-/-	-/-/-
10	T_f, °C	-/2000 /2100	2000/2100 /2200	2060/2164 /2265	2060/2164 /2265	2060/2164 /2265
11	L_1, mm	-/0.3 /2.0	-/- /0.3	-/-/-	-/-/-	-/-/-
12	L, mm	-/3.0 /4.0	1.8/2.0 /2.0	1.2/1.5 /1.8	1.0/1.2 /1.5	0.8/1.0 /1.2
13	ϑ, μm	-/24 /17	20/16 /12	10/8.5 /7.0	7.0/6.0 /5.2	6.0/5.0 /4.6
14	Ω	-/12.5 /118	90/125 /25	120/176 /260	140/200 /290	130/200 /260
15	$F_{o \cdot 10}^{-3}$, cal/cm^{3}s (at T_o=20°C)	7.5	15.3	40.7	68.2	83.5

Table 5: Dependence of thermophysical coefficients of the gas phase on the gas temperature T,°C

mixtures	T,°C	250	500	1000	1500	2000	2500
1-4	$\lambda \cdot 10^4$, cal/cm·s·K	1,6	2,0	3,2	4,4	5,6	6,7
1, 2	C_p, cal/g·K	0,34	0,35	0,38	0,415	0,45	0,48
3, 4	C_p, cal/g·K	0,365	0,38	0,415	0,44	0,47	0,50

Table 6: Influence of modifier $(C_{17}H_{35}CO_2)_2Pb$ (3% instead of oxid.) on burning wave parameters of mixture **([BAMO-AMMO]/CL-20, 20:80).** T_o=20°C. Presented as (pure mixt.)/(mixt.with modif.)

	p, MPa	0.5	1	2	5	8	10
1	m, g/m^{2}s	0.8/0.68	1.2/0.90	2.1/1.3	4.4/2.32	6.0/3.28	6.9/3.92
2	T_s, °C	285/280	302/290	325/304	360/328	375/345	382/354
3	$\varphi_{o\cdot 10}^{-4}$, °/cm	4.0/5.0	4.6/7.0	6.0/9.0	10/13	13/15	15/16
4	q, cal/g	9.0/13	7.0/14	5.4/13	4.4/11	4.3/8.8	4.3/8.0
5	q_r, cal/g	2.5/3.0	1.6/3.3	2.4/3.8	3.5/6.0	4.0/7.2	4.6/7.0
6	Q, cal/g	81/75	90/77	99/83	114/91	116/98	118/102
7	l, µm	45/50	40/45	34/40	25/30	22/24	20/22
8	l_m, µm	35/30	30/26	24/22	22/18	18/17	16/16
9	T_1, °C	1000/1000	1050/-	1100/-	1150/-	-/-	-/-
10	T_f, °C	2200/2300	2400/2400	2600/2500	2850/2630	2930/2630	2930/2630
11	L_1, mm	1.0/0.4	0.9/-	0.6/-	0.25/-	-/-	-/-
12	L, mm	5.0/3.0	5.0/2.5	4.5/3.0	4.0/2.5	3.0/3.0	2.0/2.5
13	ϑ, µm	12/13	8.4/11	4.9/7.5	2.4/4.3	2.1/6	1.8/5
14	Ω	83/31	110/236	122/400	100/580	1430/667	1100/720
15	$F_{o\cdot 10}^{-3}$, cal/cm^{3}s	-/15.7	27.5/29.5	-/55.3	178/147	-/245	479/318

Table 7: Influence of modifier $(C_{17}H_{35}CO_2)_2Pb$ (3% instead of oxid.) on burning wave parameters of mixture **([BAMO-AMMO]/HMX, 20:80).** T_o=20°C. Presented as the (pure mixt.)/(mixt. with modif.)

	p, MPa	0.5	1	2	5	8	10
1	m, g/m^2s	0.1/-	0.22/0.34	0.41/0.5	0.85/0.96	1.21/1.4	1.44/1.63
2	T_s, °C	330/-	365/392	407/425	470/477	490/497	492/505
3	$\varphi_{o\cdot 10^{-4}}$, °/cm	2.2/-	3.7/4.5	6/6	9/8	11/9	12/9.5
4	q, cal/g	46/-	37/24.5	34/25.2	26/18.5	24/15	22/13.3
5	q_r, cal/g	0.6/-	0.5/0.32	0.4/0.32	1.8/1.6	2.8/2.5	4/3.5
6	Q, cal/g	96/-	120/143	141/155	172/181	181/192	185/196
7	*l*, µm	194/-	111/70	80/60	58/40	50/35	45/30
8	l_m, µm	35/-	35/35	35/25	30/20	30/18	30/17
9	T_1, °C	900/-	1020/1000	-/-	-/-	-/-	-/-
10	T_f, °C	2000/-	2100/2000	2300/2100	2380/2164	2400/2164	2400/2164
11	L_1, mm	0.5/-	0.4/0.3	-/-	-/-	-/-	-/-
12	L, mm	2.2/-	2.0/3.0	2.2/2	2.0/1.5	1.3/1.2	0.9/1.0
13	ϑ, µm	51/-	24/24	13/16	7.0/8.5	5/6	4/5
14	Ω	9.8/-	17/12.5	169/125	286/176	360/200	225/200
15	$F_{o\cdot 10^{-3}}$, cal/cm^3s	0.9/-	3.56/7.51	-/15.3	42.1/40.7	-/68.2	89.7/83.5

Table 8: Averaged temperature profiles T(x) and heat release rate distributions F(x) in the gas phase. Mixture 1. T_0=20°C.

p, MPa	0.5		1		2		5		8		10	
m, g/cm^{2}s	0.42		0.62		1.0		2.1		2.8		3.18	
x, mm	T(x), °C	F(x) kcal/cm^{3}c	T(x), °C	F(x) kcal/cm^{3}c	T(x), °C	F(x) kcal/cm^{3}c	T(x), °C	F(x) kcal/cm^{3}c	T(x), °C	F(x) kcal/cm^{3}c	T(x), °C	F(x) kcal/cm^{3}c
0	262	8.26	276	19.7	294	35.4	320	87.8	335	146	340	223
0.05	464	7.6	591	16.3	623	29.8	753	67.8	916	141	1084	192
0.1	623	5.86	769	9.08	845	18.5	997	41.8	1420	101	1583	119
0.15	731	4.06	872	5.41	964	10.3	1193	34.2	1640	45.7	1832	57.7
0.2	805	2.61	925	2.36	1041	6.02	1339	26.6	1769	31.5	1949	31
0.3	878	1.31	953	1.19	1099	2.5	1598	22.9	1999	25.4	2129	23.4
0.4	927	0.87	1018	1.77	1145	3.62	1798	17.5	2149	17.8	2250	16.9
0.5	950	0.44	1050	1.08	1254	7.9	1949	12.4	2269	12.7	2350	12.7
0.75	1003	0.71	1153	2.05	1746	9.15	2199	8.53	2450	7.91	2510	8.02
1	1142	1.59	1401	3.3	2092	6.17	2377	5.61	2569	4.79	2610	5.08
1.25	1402	2.3	1683	3.69	2308	3.67	2480	3.9	2629	2.15	2674	2.11
1.5	1662	1.87	1976	2.8	2428	1.76	2575	2.85	2650	0.85	2675	0
2	1986	1.17	2234	1.35	2521	0.61	2668	9.63	2674	0.34		
2.5	2210	0.79	2407	0.84	2546	0.13	2675	0	2675	0		
3	2342	0.34	2488	0.29	2550	0						
4	2396	0.05	2500	0								
4.5	2400	0										

`

Table 9: Averaged temperature profiles T(x) and heat release rate distributions F(x) in the gas phase. Mixture 2. T_0=20°C

p, MPa	0.5		1		2		5		8		10	
m, g/cm^{2}s	0.68		0.9		1.3		2.3		3.32		3.92	
x, mm	T(x), °C	F(x) kcal/cm^{3}c	T(x), °C	F(x) kcal/cm^{3}c	T(x), °C	F(x) kcal/cm^{3}c	T(x), °C	F(x) kcal/cm^{3}c	T(x), °C	F(x) kcal/cm^{3}c	T(x), °C	F(x) kcal/cm^{3}c
0	280	15.7	290	29.5	304	55.3	328	147	345	245	354	318
0.05	514	14.7	613	25.8	750	56.3	971	137	1085	213	1152	270
0.1	712	12.0	854	19.1	1176	50	1483	97	1602	134	1683	165
0.15	851	8.01	1032	14.6	1474	32.3	1742	48.9	1853	65.9	1953	86.0
0.2	935	4.95	1171	11.6	1632	17.4	1879	30	1989	40.9	2106	50.3
0.25	995	3.83	1279	9.34	1734	11.6	1997	24.9	2096	28.9	2199	32.8
0.3	1048	3.92	1375	8.16	1800	8.4	2079	16.1	2150	18.3	2269	22.6
0.4	1189	5.49	1527	6.34	1926	7.1	2180	10.8	2268	14.9	2349	13.3
0.5	1369	5.59	1646	4.59	1999	4.0	2259	7.73	2320	7.9	2400	9.04
0.75	1684	3.62	1837	3.15	2120	3.17	2380	5.23	2429	6.1	2499	6.09
1	1878	2.17	1985	2.47	2238	2.9	2478	3.84	2499	3.73	2550	4.0
1.25	1998	1.41	2102	1.93	2333	2.13	2539	2.39	2541	2.98	2598	3.2
1.5	2082	0.98	2195	1.51	2395	1.27	2578	1.31	2588	2.31	2627	1.17
2	2192	0.62	2332	0.92	2463	0.56	2610	0.6	2628	0.69	2630	0
2.5	2261	0.35	2389	0.27	2481	0.21	2629	0.25	2630	0		
3	2291	0.11	2400	0	2497	0.13	2630	0				
3.5	2300	0			2500	0						

Table 10: Averaged temperature profiles T(x) and heat release rate distributions F(x) in the gas phase. Mixture 3. $T_0=20^oC$

p, MPa	1		2		5		8		10	
m, g/cm^2s	0.26		0.4		0.73		1.0		1.16	
x, mm	T, ^oC	F, kcal/cm^3s	T, ^oC	F, kcal/cm^3s	T, ^oC	F, kcal/cm^3s	T, ^oC	F, kcal/cm^3s	T, ^oC	F, kcal/cm^3s
0	375	3.98	408	8.04	456	23.9	480	43.3	488	57
0.05	520	3.75	594	7.08	791	27.0	873	38.8	956	55.9
0.1	628	2.85	689	3.83	1180	27.4	1187	30.9	1373	44.7
0.15	714	2.39	769	3.33	1369	12.8	1432	23.5	1590	22.8
0.2	759	1.16	829	2.51	1491	8.68	1593	15.4	1715	13.9
0.25	789	0.845	870	1.75	1547	3.83	1710	11.7	1798	9.52
0.3	810	0.555	910	1.65	1580	2.45	1794	7.75	1859	7.0
0.4	840	0.4	969	1.15	1640	2.28	1896	4.7	1949	5.05
0.5	860	0.304	1000	0.55	1690	1.84	1959	3.02	2010	3.61
0.75	919	0.301	1041	0.49	1790	1.67	2074	1.93	2139	2.21
1	960	0.227	1129	1.45	1899	1.62	2125	0.8	2168	0.44
1.25	998	0.19	1422	2.68	1989	1.36	2149	0.43	2170	0
1.5	1029	0.308	1733	1.99	2066	1.04	2164	0.2		
2	1224	0.848	1934	0.6	2161	0.43	2170	0		
2.5	1642	0.983	1997	0.16	2170	0				
3	1843	0.38	2000	0						
3.5	1895	0.077								
4.0	1900	0								

Table 11: Averaged temperature profiles T(x) and heat release rate distributions F(x) in the gas phase. Mixture 4. $T_0=20^oC$

p, MPa	1		2		5		8		10	
m, g/cm^2s	0.34		0.5		0.96		1.37		1.64	
x, mm	T, ^oC	F, kcal/ cm^3s	T, ^oC	F, kcal/ cm^3s	T, ^oC	F, kcal/ cm^3s	T, ^oC	F, kcal/ cm^3s	T, ^oC	F, kcal/ cm^3s
0	392	7.51	425	15.3	477	40.7	497	68.2	505	83.5
0.05	605	7.17	723	15.0	853	34.0	934	53.7	953	65.9
0.1	782	5.91	996	13.9	1099	22.2	1162	30.7	1211	38.2
0.15	898	3.79	1233	11.9	1272	16.1	1325	22.4	1381	27.6
0.2	962	2.07	1372	6.7	1395	11.7	1447	17.3	1517	22.2
0.25	999	1.22	1460	4.46	1485	8.55	1544	12.7	1625	18.8
0.3	1028	1.2	1510	2.48	1549	6.1	1601	8.5	1727	16.1
0.4	1140	2.2	1599	2.38	1649	4.88	1720	9.2	1869	11.1
0.5	1257	2.03	1678	1.98	1730	4.12	1839	7.6	1969	7.35
0.75	1488	1.47	1827	1.43	1916	3.35	2019	4.44	2119	3.66
1	1630	0.92	1927	1.0	2035	2.13	2120	2.31	2162	0.87
1.25	1731	0.67	2005	0.76	2113	1.29	2161	0.75	2164	0
1.5	1806	0.48	2059	0.42	2154	0.47	2164	0		
2	1903	0.30	2095	0.1	2164	0				
2.5	1965	0.17	2100	0						
3	1992	0.06								
3.5	2000	0								

Table 12: Temperature sensitivities of burning rate (**β**,1/^{o}) and surface temperature (**r**), and criteria of stable combustion k and k*.
Mixtures 1 – 4, and mixtures (*) and (**) without modifier.

Presented at T_o: -100^{o}C /20^{o}C /100^{o}C.

mixt.	p, MPa	0.5	1	2	5	8	10
№ 1	**r**	0.017/0.08 /0.16	0.033/0.075 /0.11	0.033/0064 /0.075	0.042/0.05 /0.063	0.075/0.05 /0.038	0.067/0.05 /0.038
(BAMO-THF)/	**β**·10^3, 1/^{o}	0.35/2.2 /4.6	1.3/1.8 /3.2	1.3/1.8 /3.2	1.3/1.3 /1.3	1.3/1.3 /1.3	1.3/1.3 /1.3
HNIW, 20:80	**k**	0.126/0.53 /0.8	0.48/0.46 /0.59	0.5/0.4 /0.32	0.54/0.39 /0.29	0.55/0.4 /0.3	0.56/0.42 /0.31
№ 2	**r**	0.07/0.06 /0.05	0.07/0.05 /0.04	0.05/0.045 /0.03	0.04/0.045 /05.5	0.04/0.04 /0.04	0.05/0.045 /0.04
(BAMO-AMMO)/	**β**·10^3, 1/^{o}	-/1.85 /1.7	1.85/1.5 /1.15	1.4/1.0 /0.5	0.9/0.9 /0.9	0.85/0.85 /0.85	0.85/0.85 /0.85
HNIW+ Pb stear.	**k**	-/0.48 /0.31	0.7/0.4 /0.22	0.56/0.28 /0.1	0.38/0.28 /0.2	0.37/0.28 /0.21	0.38/0.28 /0.22
№ 3	**r**	-/- /-	0.18/0.34 /0.5	0.19/0.3 /0.44	0.11/0.2 /0.3	0.11/0.15 /0.18	0.11/0.13 /0.15
(BAMO-THF)/	**β**·10^3, 1/^{o}	-/- /-	3.1/4.6 /6.9	2.6/4.0 /5.5	2.2/3.1 /4.0	1.8/2.6 /3.3	1.7/2.5 /3.2
HMX, 20:80	**k**	-/- /-	1.4/1.63 /2.17	1.26/1.55 /1.89	1.2/1.35 /1.52	1.0/1.2 /1.3	0.98/1.17 /1.28
	k*	-/- /-	0.36/0.45 /0.87	0.16/0.4 /0.63	0.16/0.25 /0.36	-/0.12 /0.22	-/0.097 /0.23
№ 4	**r**	-/- /-	0.18/0.24 /0.3	0.17/0.22 /0.3	0.12/0.14 /0.16	0.09/0.095 /0.1	0.08/0.075 /0.07
(BAMO-AMMO)/	**β**·10^3, 1/^{o}	-/- /-	2.9/3.35 /3.7	1.85/3.0 /4.0	1.5/2.7 /2.9	1.9/1.9 /1.9	1.9/1.9 /1.9
HMX+ Pb stear.	**k**	-/- /-	1.36/1.25 /1.17	0.93/1.2 /1.4	0.84/1.23 /1.13	1.11/0.9 /0.77	1.13/0.92 /0.78
	k*	-/- /-	0.3/0.11 /0.045	-/0.08 /0.22	-/0.17 /0.05	0.06/- /-	0.097/- /-
(*)	**r**	-/0.13 /0.18	0.20/0.15 /0.13	0.20/0.15 /0.09	0.22/0.18 /0.07	0.24/0.18 /0.09	0.24/0.20 /0.15
(BAMO-AMMO)/	**β**·10^3, 1/^{o}	-/2.8 /4.0	5.6/3.0 /3.0	4.7/3.6 /2.3	4.2/3.0 /1.6	4.2/3.0 /1.8	4.0/2.8 /2.0
HNIW, 20:80	**k**	-/0.74 /0.79	2.13/0.85 /0.64	1.87/1.1 /0.53	1.8/1.02 /0.42	1.8/1.12 /0.5	1.8/1.0 /0.98
	k*	-/- /-	**2.0**/- /-	**1.3**/0.7 /-	**1.03**/- /-	0.9/- /-	0.2/- /-
(**)	**r**	-/- /-	0.17/0.19 /0.21	0.14/0.16 /0.175	0.08/0.12 /0.14	0.065/0.066 /0.07	0.067/0.067 /-
(BAMO-AMMO)/	**β**·10^3, 1/^{o}	-/- /-	2.76/2.76 /2.76	1.96/1.96 /1.96	1.36/1.6 /1.84	1.15/1.3 /1.5	1.2/1.2 /-
HMX, 20:80	**k**	-/- /-	1.23/0.95 /0.8	0.96/0.759 /0.645	0.76/0.72 /0.72	0.67/0.61 /0.61	0.71/0.576 /-
	k*	-/- /-	0.14/- /-	-/- /-	-/- /-	-/- /-	-/- /-

Table 13: Characteristics of erosive combustion.
Mixtures 1 – 4, and mixtures (*) and (**) without modifier.
Rough burning surface. T_o=20°C.

mixt.	p, MPa	m_o, g/cm^{2}s /T_{so}, °C	W, m/s											
			100			300			600			800		
			ε	m, g/cm^{2}s	T_s, °C	ε	m, g/cm^{2}s	T_s, °C	ε	m, g/cm^{2}s	T_s, °C	ε	m, g/cm^{2}s	T_s, °C
№ 1 (BAMO-THF)/ HNIW, 20:80	1	0.62/ 276	1.09	0.68	279	1.13	0.70	280	1.44	0.89	290	1.63	1.01	295
	5	1.92/ 320	1.05	2.02	322	1.19	2.28	328	1.72	3.30	347	2.04	3.92	356
	10	2.98/ 340	1.02	3.04	343	1.24	3.70	353	2.11	6.29	380	2.54	7.57	389
№ 2 (BAMO-AMMO)/ HNIW+ Pb stear.	1	0.9/ 290	1.06	0.96	292	1.08	0.97	293	1.26	1.14	299	1.44	1.30	304
	5	2.32/ 328	1.03	2.38	329	1.25	2.89	340	1.74	4.04	357	2.00	4.63	364
	10	3.92/ 354	1.00	3.92	354	1.27	4.96	368	1.79	7.02	383	2.12	8.30	395
№ 3 (BAMO-THF)/ HMX, 20:80	1	0.26/ 375	1.91	0.50	425	2.49	0.65	445	3.43	0.89	470	4.08	1.06	485
	5	0.73/ 455	1.98	1.44	505	2.94	2.15	520	4.11	3.00	544	4.99	3.64	554
	10	1.16/ 488	2.11	2.45	533	3.38	3.92	558	4.95	5.74	580	5.84	6.77	590
№ 4 (BAMO-AMMO)/ HMX+ Pb stear.	1	0.34/ 392	1.67	0.57	435	1.94	0.66	448	2.60	0.88	470	3.07	1.04	484
	5	0.96/ 477	1.73	1.66	508	2.41	2.31	522	3.39	3.25	548	3.92	3.76	556
	10	1.63/ 505	2.17	3.54	553	2.62	4.27	563	3.69	6.01	583	4.37	7.12	593
(*) (BAMO-AMMO)/ HNIW, 20:80	1	1.2/ 301	1.04	1.25	302	1.05	1.26	303	1.12	1.34	305	1.23	1.48	309
	5	4.4/ 360	1.00	4.4	360	1.00	4.4	360	1.06	4.66	364	1.19	5.24	371
	10	6.9/ 382	1.00	6.9	382	1.00	6.9	382	1.18	8.14	393	1.41	9.73	403
(**) (BAMO-AMMO)/ HMX, 20:80	1	0.22/ 365	1.51	0.33	392	2.11	0.46	416	3.10	0.68	450	3.66	0.81	466
	5	0.85/ 470	1.88	1.60	508	2.44	2.07	518	3.27	2.78	540	3.77	3.20	547
	10	1.44/ 500	1.79	2.58	536	2.71	3.90	558	3.88	5.59	578	4.56	6.57	588

Table 14: Sensitivities of burning rates and surface temperatures to pressure and initial sample temperature.
Mixtures 1 – 4, and mixtures (*) and (**) without modifier. T_o=20°C.

	p, MPa	0.5	1	2	5	8	10
mixtures	property						
№ 1	•	0.56	0.62	0.68	0.68	0.68	0.68
(BAMO-THF)/ HNIW, 20:80	**r**	0.08	0.075	0.06	0.05	0.05	0.05
	k	0.53	0.46	0.40	0.39	0.40	0.416
	$\mu \cdot 10^2$	6.8	8.65	9.98	10.13	8.68	5.43
№ 2	•	0.41	0.47	0.58	0.70	0.77	0.77
(BAMO-AMMO)/ HNIW+ Pb stear.	**r**	0.06	0.05	0.045	0.045	0.040	0.045
	k	0.48	0.40	0.28	0.28	0.276	0.28
	$\mu \cdot 10^2$	5.0	6.1	7.64	10.3	11.8	11.8
№ 3	•	-	0.65	0.65	0.65	0.65	0.65
(BAMO-THF)/ HMX, 20:80	**r**	-	0.34	0.33	0.25	0.16	0.13
	k	-	1.63	1.55	1.35	1.20	1.17
	$\mu \cdot 10^2$	-	12.2	12.5	11.9	9.4	6.5
№ 4	•	-	0.56	0.66	0.75	0.75	0.75
(BAMO-AMMO)/ HMX+ Pb stear.	**r**	-	0.24	0.22	0.14	0.095	0.075
	k	-	1.246	1.20	1.23	0.9	0.92
	$\mu \cdot 10^2$	-	12.1	12.4	11.2	7.9	6.8
(*)	•	0.55	0.70	0.82	0.73	0.68	0.68
(BAMO-AMMO)/ HNIW, 20:80	**r**	0.13	0.15	0.15	0.18	0.18	0.20
	k	0.74	0.85	1.10	1.02	1.12	1.01
	$\mu \cdot 10^2$	0.10	0.12	0.115	0.11	0.10	0.10
(**)	•	-	0.90	0.82	0.80	0.79	0.79
(BAMO-AMMO)/ HMX, 20:80	**r**	-	0.19	0.16	0.105	0.066	0.067
	k	-	0.95	0.76	0.72	0.61	0.576
	$\mu \cdot 10^2$	-	0.174	0.168	0.11	0.094	0.092

Table 15: Pressure-coupled burn-rate response function characteristics. Mixtures 1 - 4. T_o=20°C.

		Properties									
Systems	p, MPa	$\mathbf{Re\{U\}_m}$	ω_n	ϖ_n, kHz	$\mathbf{Re\{U\}_{20}}$	Im {U} max+	ω_{im+}	ϖ_{im+}, Hz	Im {U} min	ω_{im-}	ϖ_{im-}, kHz
(BAMO-THF)/ HNIW 20:80	0.5	0.79	6.5	0.23	0.72	0.095	1	35	-0.135	20	0.7
	1	0.82	7	0.48	0.76	0.083	1	70	-0.136	20	1.4
	2	0.86	6.5	1.0	0.81	0.075	1	150	-0.13	20	3.0
	5	0.86	7	3.0	0.81	0.073	1	420	-0.127	20	8.4
	8	0.876	7	5.1	0.836	0.079	1	730	-0.111	20	15
	10	0.916	10	9.0	0.898	0.094	1	900	-0.07	20	18
(AMMO-BAMO)/ HNIW+ +stearate of Pb	0.5	0.562	7.5	0.7	0.53	0.062	1	90	-0.085	20	1.9
	1	0.604	7	0.9	0.577	0.055	1	125	-0.078	20	2.5
	2	0.684	7	1.5	0.663	0.042	1	210	-0.061	20	4.2
	5	0.82	7	3.4	0.79	0.05	0.9	440	-0.083	20	6.7
	8	0.9	6.5	5.8	0.865	0.053	1	900	-0.094	20	17.8
	10	0.9	7	8.0	0.864	0.054	0.9	1020	-0.096	20	22.7
(BAMO-THF)/ HMX	1	2.55	3.5	0.07	0.436	0.79	1.9	36	-1.2	6	0.1
	2	2.187	3.5	0.14	0.452	0.63	1.5	62	-1.0	6.5	0.3
	5	1.846	4.1	0.40	0.543	0.488	1.7	165	-0.82	9	0.9
	8	1.86	6	1.04	0.866	0.487	2	350	-0.812	15	2.6
	10	2.08	8	1.80	1.287	0.59	2.8	640	-0.82	20	4.5
(AMMO-BAMO)/ HMX+ +stearate of Pb	1	1.31	3.9	0.1	0.396	0.3	1.3	37	-0.6	10	0.3
	2	1.55	4	0.2	0.6	0.36	1.5	75	-0.66	11	0.6
	5	2.48	6.5	0.9	1.03	0.65	2.5	350	-1.19	16	2.3
	8	1.605	8	1.9	1.34	0.344	2	460	-0.48	20	4.6
	10	1.78	10	3.2	1.6	0.407	2.4	770	-0.468	20	6.4

Table 16: Characteristics of pressure-coupled burn-rate response function of mixtures without modifier. T_o=20°C.

Systems	p, MPa	Properties									
		$\mathbf{Re\{U\}_m}$	ω_n	ϖ_n, *KHz*	$\mathbf{Re\{U\}_{20}}$	Im {U} max+	ω_{im+}	ϖ_{im+}, KHz	Im {U} min	ω_{im-}	ϖ_{im-}, KHz
(AMMO-BAMO)/ HNIW, 20:80	0.5	0.86	4.5	0.45	0.75	0.13	1.0	0.10	-0.26	17	1.72
	1	1.21	4.75	0.81	0.80	0.21	1.25	0.21	-0.39	18	3.1
	2	2.03	6.0	2.12	1.20	0.49	1.75	0.62	-0.80	17	6.0
	5	1.51	4.75	5.9	0.80	0.32	1.5	1.88	-0.52	15	18.8
	8	1.62	5.0	9.7	0.80	0.39	1.75	3.4	-0.60	14	27
	10	1.36	4.5	10.6	0.80	0.29	1.25	2.95	-0.40	13	30
(AMMO-BAMO)/ HMX, 20:80	1	1.62	4.0	0.05	0.95	0.29	1.0	0.014	-0.59	15	0.20
	2	1.26	4.0	0.12	0.95	0.18	1.0	0.03	-0.40	15	0.45
	5	1.31	6.0	0.52	0.80	0.21	1.25	0.11	-0.30	18	1.55
	8	1.22	8.0	1.18	0.79	0.17	1.25	0.19	-0.18	18	2.66
	10	1.18	7.75	1.44	0.79	0.16	1.0	0.19	-0.16	20	3.72

Table 17: Coefficients of erosive combustion ε for smooth burning surfaces. T_o=20°C.

			W, m/s			
mixtures	p, MPa	m_o, g/cm^{2}s /T_{so}, °C	100	300	600	800
№ 1 (BAMO-THF)/ HNIW, 20:80	1	0.62/ 276	1.07	1.14	1.42	1.56
	5	1.92/ 320	1.0	1.17	1.54	1.78
	10	2.98/ 340	1.0	1.37	1.91	2.13
№ 2 (BAMO-AMMO)/ HNIW+ Pb stear.	1	0.9/ 290	1.07	1.1	1.26	1.4
	5	2.32/ 328	1.04	1.22	1.62	1.76
	10	3.92/ 354	1.0	1.23	1.66	1.82
№ 3 (BAMO-THF)/ HMX, 20:80	1	0.26/ 375	1.90	2.43	3.08	3.56
	5	0.73/ 455	1.96	2.63	3.51	4.02
	10	1.16/ 488	2.3	2.86	3.9	4.48
№ 4 (BAMO-AMMO)/ HMX+ Pb stear.	1	0.34/ 392	1.67	1.9	2.4	2.7
	5	0.96/ 477	1.73	2.18	2.85	3.24
	10	1.63/ 505	2.16	2.32	3.05	3.47
(*) (BAMO-AMMO)/ HNIW, 20:80	1	1.2/ 301	1.01	1.035	1.11	1.21
	5	4.4/ 360	1.02	1.04	1.14	1.24
	10	6.9/ 382	1.03	1.08	1.2	1.29
(**) (BAMO-AMMO)/ HMX, 20:80	1	0.22/ 365	1.5	2.0	2.8	3.16
	5	0.85/ 470	1.85	2.3	2.9	3.3
	10	1.44/ 500	1.75	2.4	3.1	3.6

Table 18: Characteristics of velocity-coupled burn-rate response functions of the studied mixtures. T_o=20°C.

	p, MPa	1		5		10	
mixtures	W_o, m/s	300	600	300	600	300	600
№ 1	$Re\{V_w\}_{max}$	0.235	0.46	0.305	0.61	0.58	0.51
(BAMO-THF)/ HNIW, 20:80	$\omega_{Re\,max}$	1	1	1	1	1	1
	ϖ, kHz	0.09	0.135	0.56	0.97	1.67	3.25
	$\omega_n=\sqrt{k_w}/r_w$	9.5	8.4	10.3	8.7	9.0	7.4
№ 2	$Re\{V_w\}_{max}$	0.115	0.385	0.325	0.445	0.38	0.47
(BAMO-AMMO)/ HNIW+ Pb stear.	$\omega_{Re\,max}$	1	1	1	1	1	1
	ϖ, kHz	0.15	0.20	0.75	1.3	1.7	3.1
	$\omega_n=\sqrt{k_w}/r_w$	10.3	9.6	11.7	10	11.5	9.6
№ 3	$Re\{V_w\}_{max}$	0.3	0.42	8.3	0.44	0.28	0.48
(BAMO-THF)/ HMX, 20:80	$\omega_{Re\,max}$	1	1	4	1	1	1
	ϖ, kHz	0.12	0.19	0.68	1.28	1.84	3.4
	$\omega_n=\sqrt{k_w}/r_w$	2.65	2.3	4.9	4.1	5.0	4.2
№ 4	$Re\{V_w\}_{max}$	0.5	1.63	0.84	0.4	0.28	0.88
(BAMO-AMMO)/ HMX+ Pb stear.	$\omega_{Re\,max}$	3	4	4	1	3	5
	ϖ, kHz	0.315	0.67	2.68	1.15	5.07	14.5
	$\omega_n=\sqrt{k_w}/r_w$	3.5	3.04	5.76	9.84	9.76	`9.68
(*)	$Re\{V_w\}_{max}$	0.08	0.265	0.07	0.32	0.125	0.33
(BAMO-AMMO)/ HNIW, 20:80	$\omega_{Re\,max}$	1	1	1	1	1	1
	ϖ, kHz	0.185	0.218	1.35	1.62	2.75	3.4
	$\omega_n=\sqrt{k_w}/r_w$	7.42	7.0	6.72	6.38	6.93	6.5
(**)	$Re\{V_w\}_{max}$	0.56	1.2	0.35	0.6	0.39	0.6
(BAMO-AMMO)/ HMX, 20:80	$\omega_{Re\,max}$	2	3	2	3	1	2
	ϖ, kHz	0.1	0.26	0.92	2.28	1.04	3.64
	$\omega_n=\sqrt{k_w}/r_w$	3.9	5.8	7.35	6.35	7.94	6.77

FIGURES of Final Report, N62558-03-M-0812

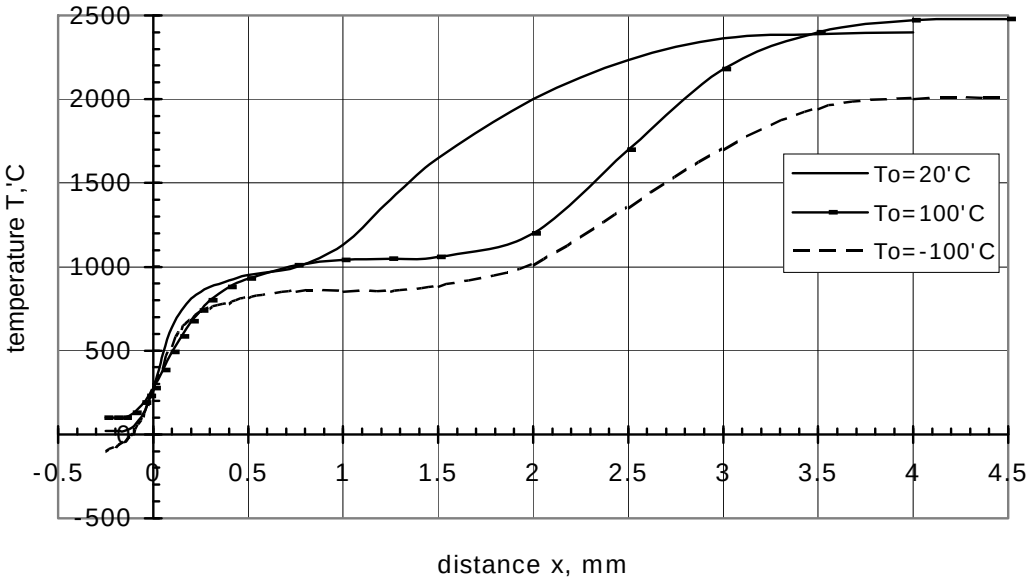

Figure 1: Averaged temperature profiles T(x) of mixture 1 [(BAMO-THF)/HNIW, (20:80)] at 0.5 MPa and various To.

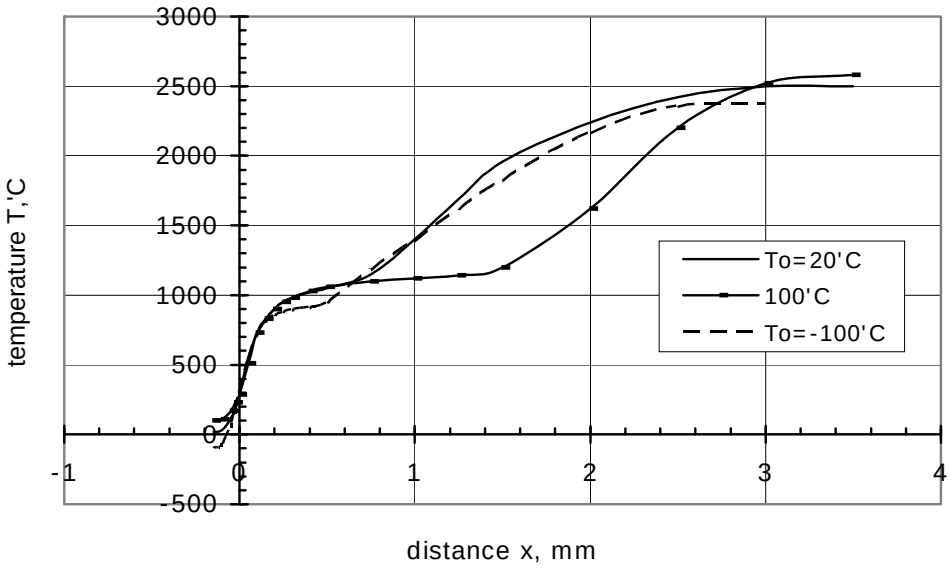

Figure 2: Averaged temperature profiles T(x) of mixture 1 [(BAMO-THF)/HNIW, (20:80)] at 1 MPa and various To.

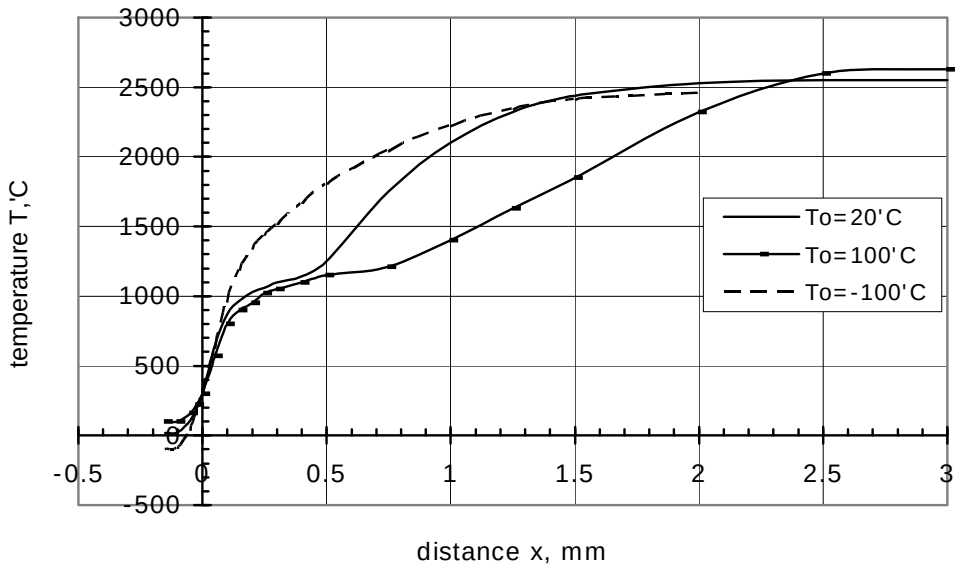

Figure 3: Averaged temperature profiles T(x) of mixture 1 [(BAMO-THF)/HNIW, (20:80)] at 2 MPa and various To.

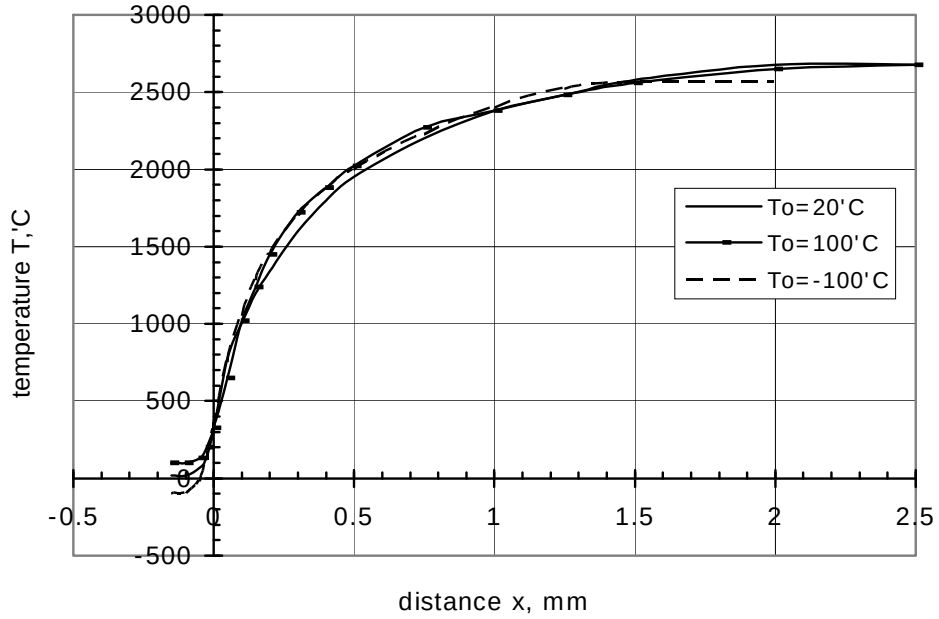

Figure 4: Averaged temperature profiles T(x) of mixture 1 [(BAMO-THF)/HNIW, (20:80)] at 5 MPa and various To.

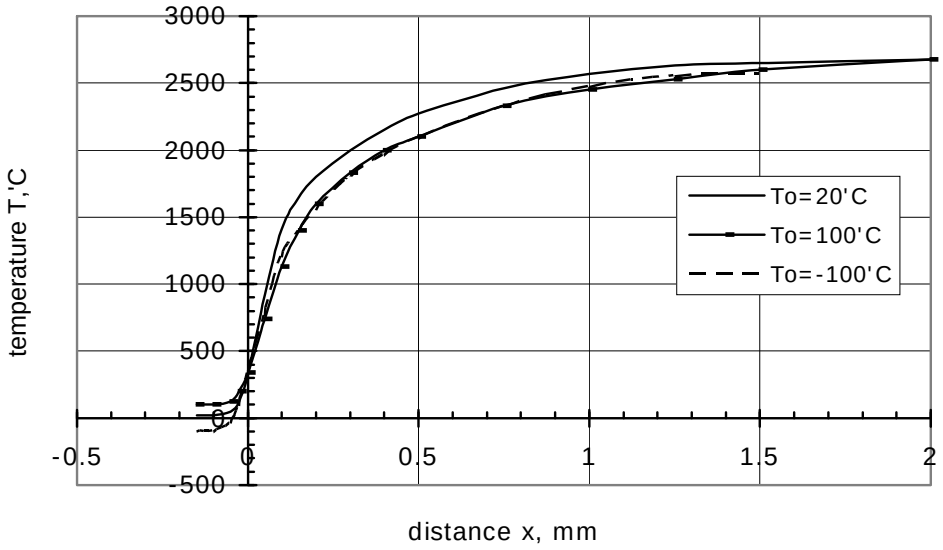

Figure 5: Averaged temperature profiles T(x) of mixture 1 [(BAMO-THF)/HNIW, (20:80)] at 8 MPa and various To.

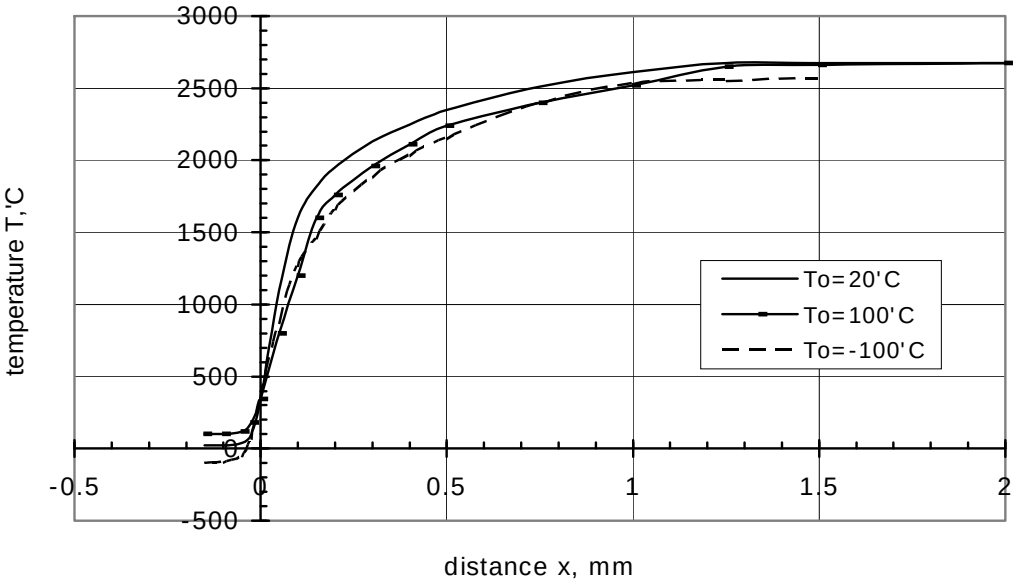

Figure 6: Averaged temperature profiles T(x) of mixture 1 [(BAMO-THF)/HNIW, (20:80)] at 10 MPa and various To.

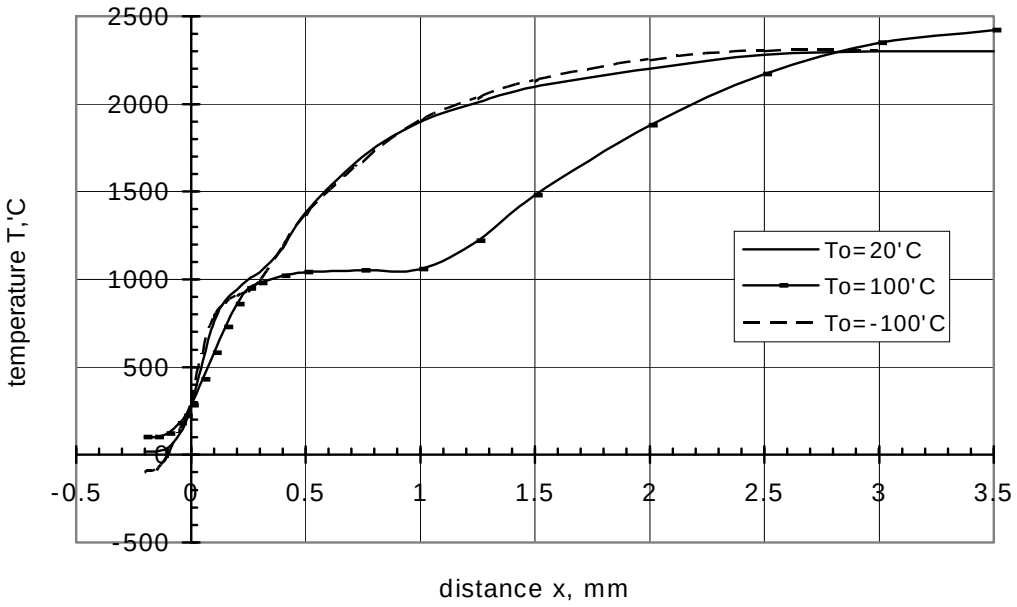

Figure 7: Averaged temperature profiles T(x) of mixture 2 [(BAMO-AMMO)/HNIW+stear.Pb, (20:77:3)] at 0.5 MPa and various To.

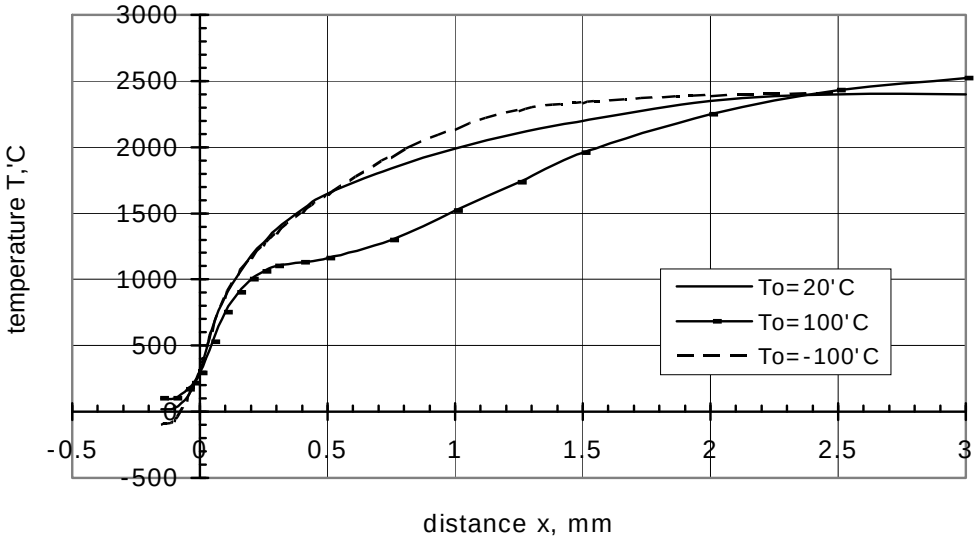

Figure 8: Averaged temperature profiles T(x) of mixture 2 [(BAMO-AMMO)/HNIW+stear.Pb, (20:77:3)] at 1 MPa and various To.

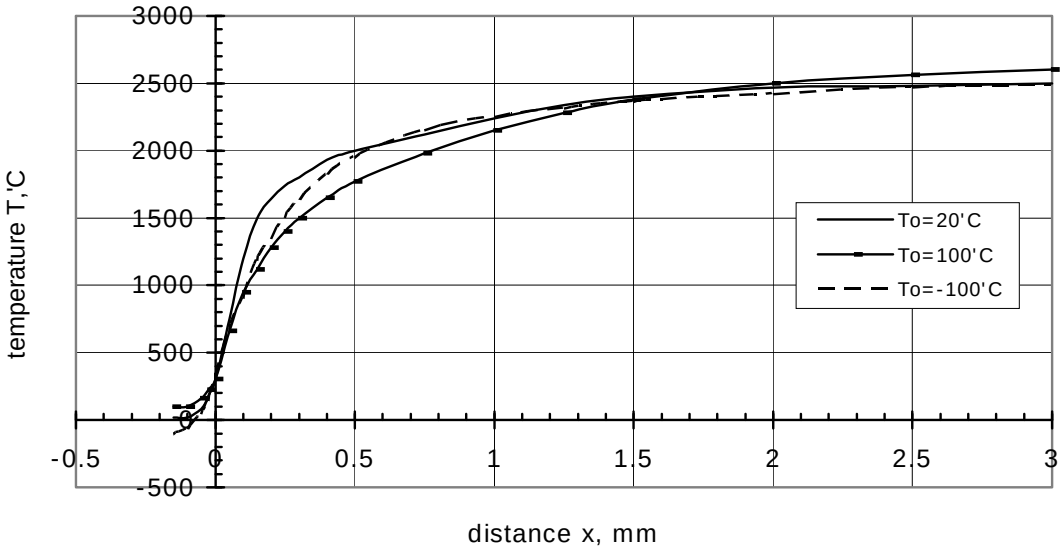

Figure 9: Averaged temperature profiles T(x) of mixture 2 [(BAMO-AMMO)/HNIW+stear.Pb, (20:77:3)] at 2 MPa and various To.

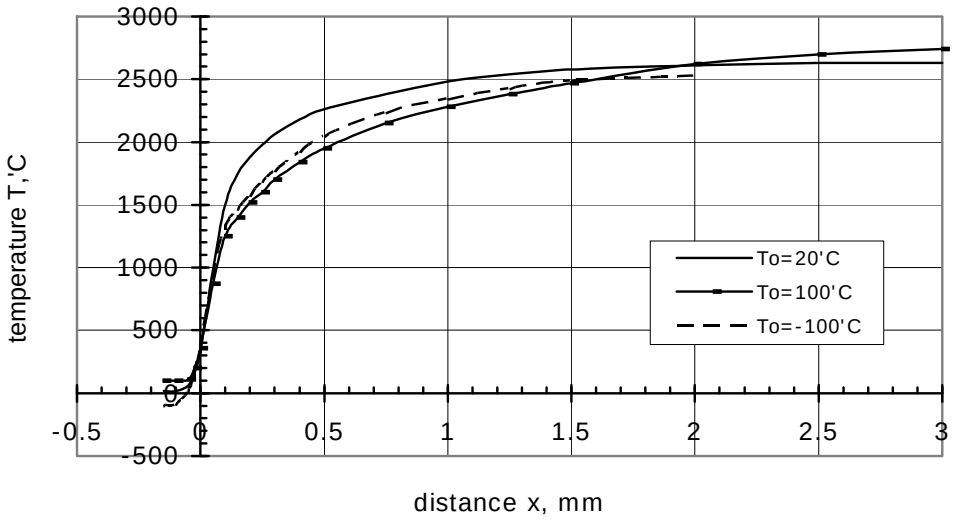

Figure 10: Averaged temperature profiles T(x) of mixture 2 [(BAMO-AMMO)/HNIW+stear.Pb, (20:77:3)] at 5 MPa and various To.

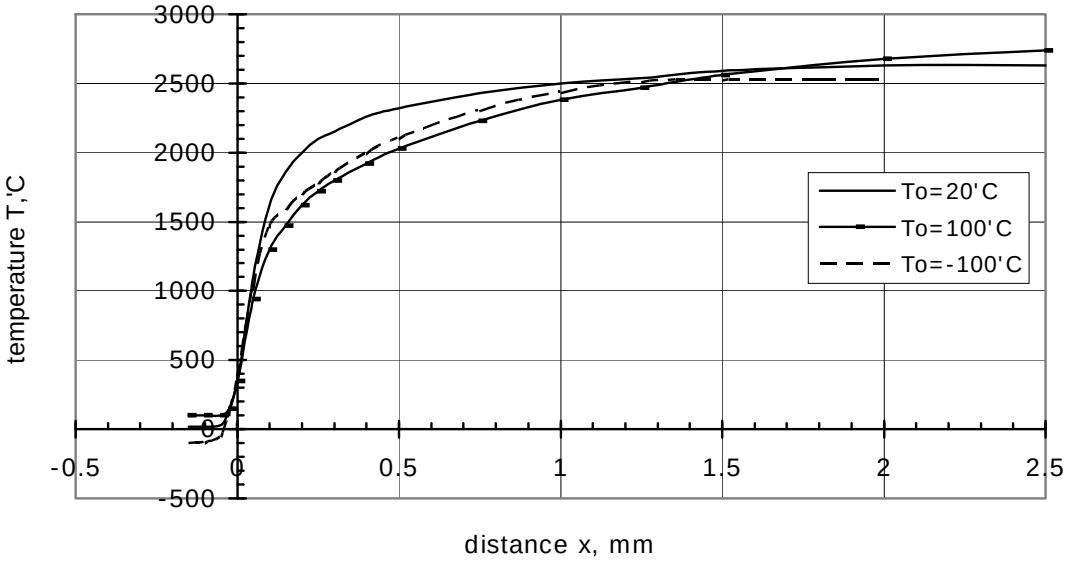

Figure 11: Averaged temperature profiles T(x) of mixture 2 [(BAMO-AMMO)/HNIW+stear.Pb, (20:77:3)] at 8 MPa and various To.

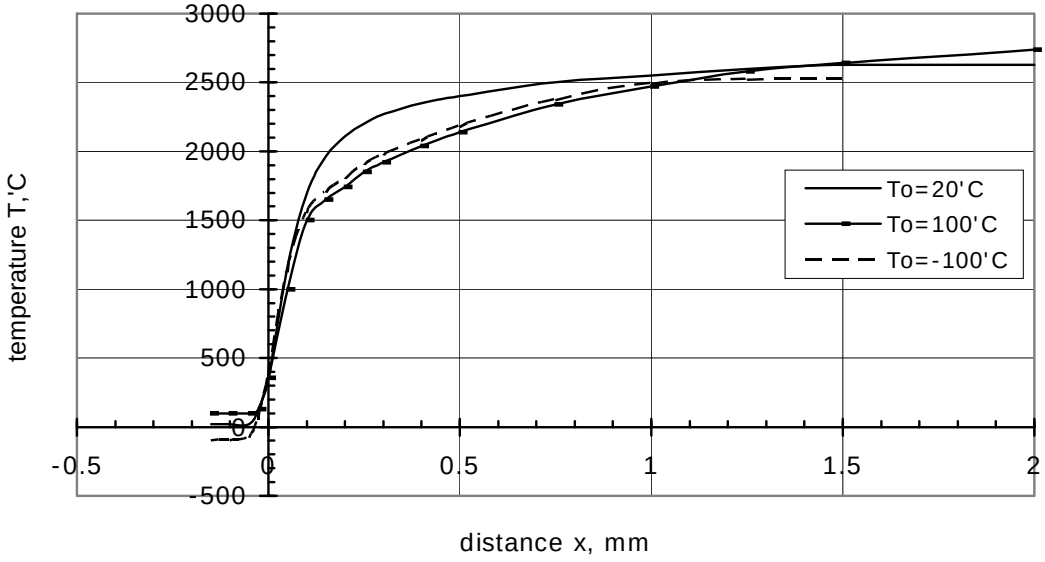

Figure 12: Averaged temperature profiles T(x) of mixture 2 [(BAMO-AMMO)/HNIW+stear.Pb, (20:77:3)] at 10 MPa and various To.

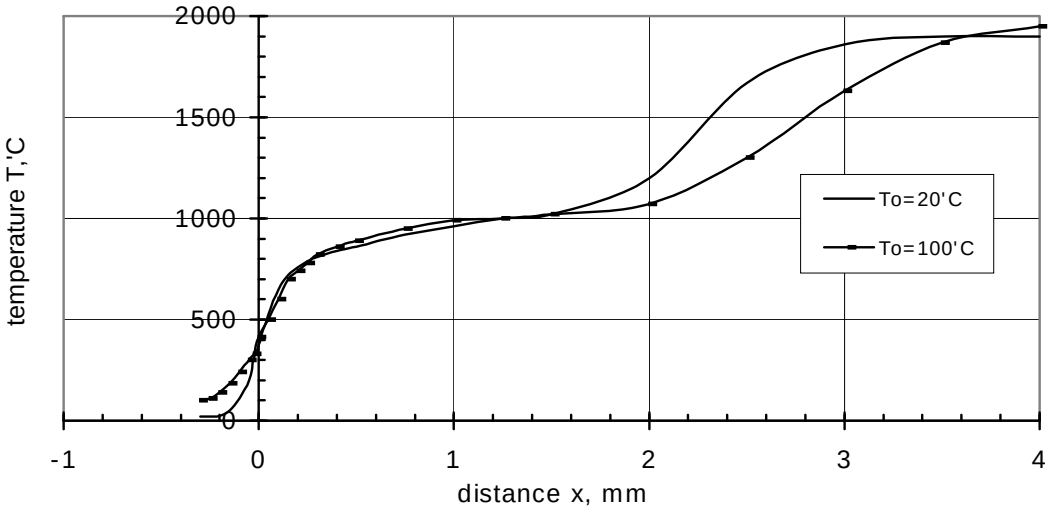

Figure 13: Temperature profiles T(x) of mixture 3 [(BAMO-THF)/HMX, (20:80)] at 1 MPa and various To.

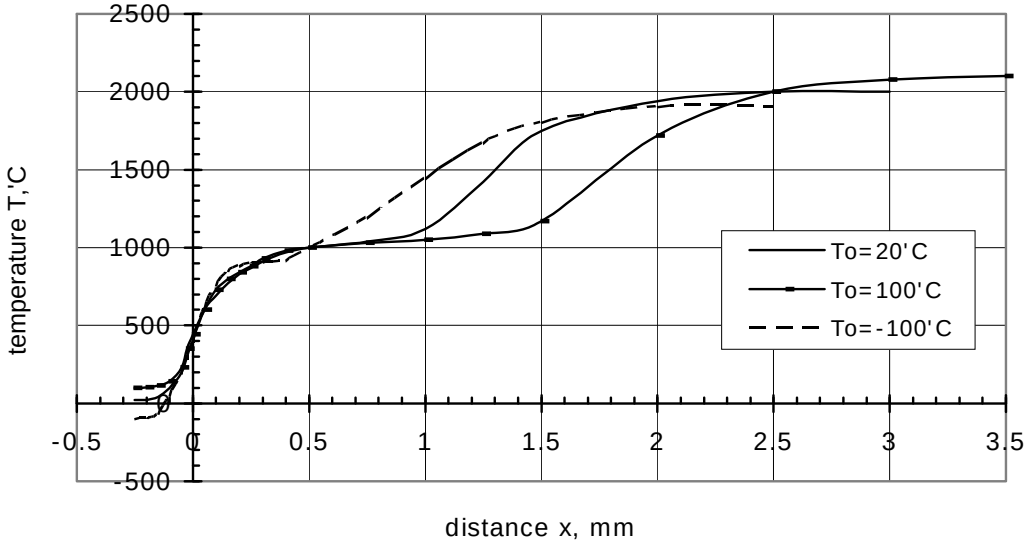

Figure 14: Averaged temperature profiles T(x) of mixture 3 [(BAMO-THF)/HMX, (20:80)] at 2 MPa and various To.

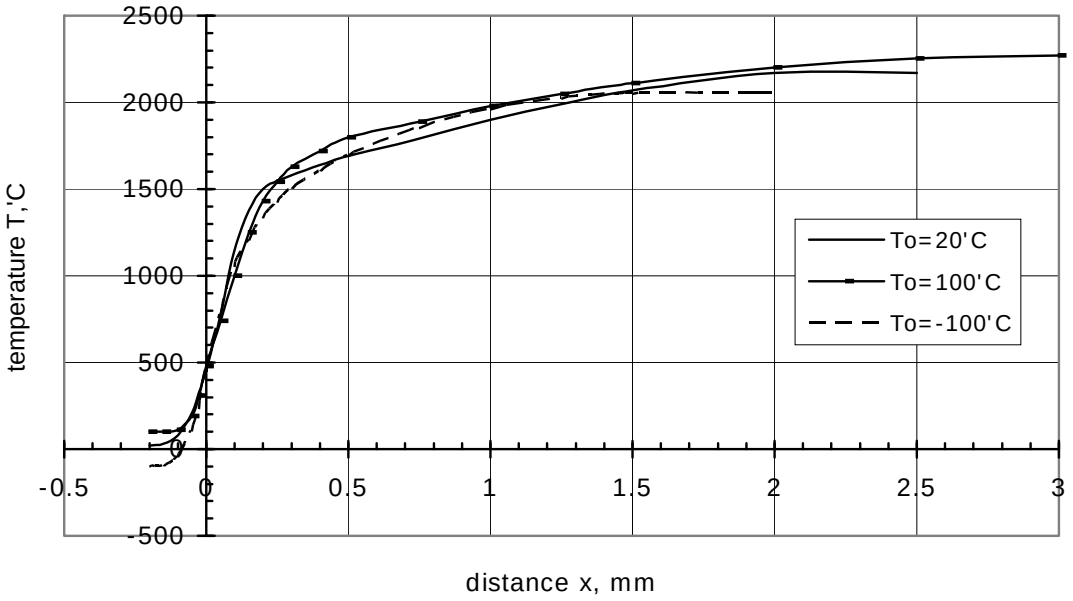

Figure 15: Averaged temperature profiles T(x) of mixture 3 [(BAMO-THF)/HMX, (20:80)] at 5 MPa and various To.

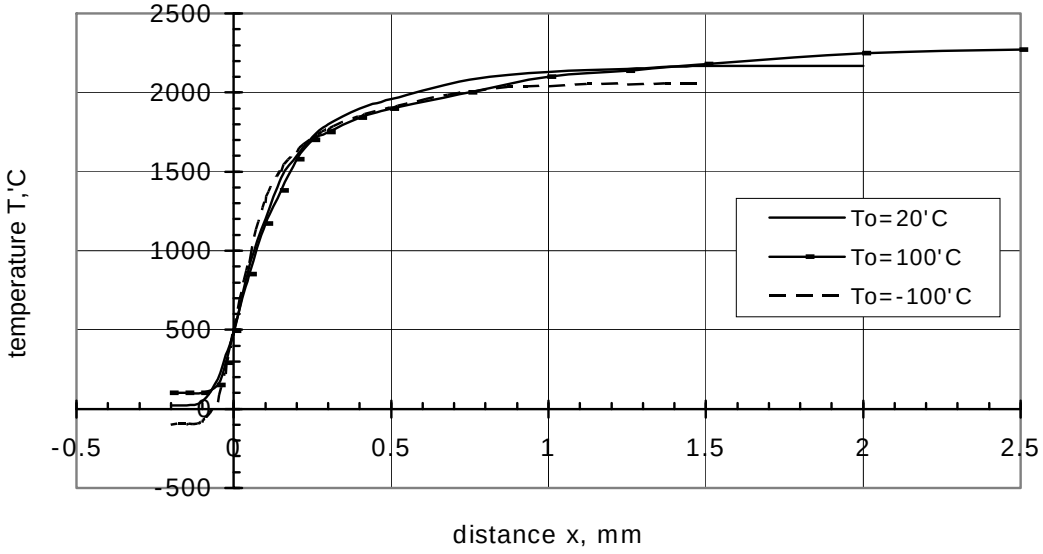

Figure 16: Averaged temperature profiles T(x) of mixture 3 [(BAMO-THF)/HMX, (20:80)] at 8 MPa and various To.

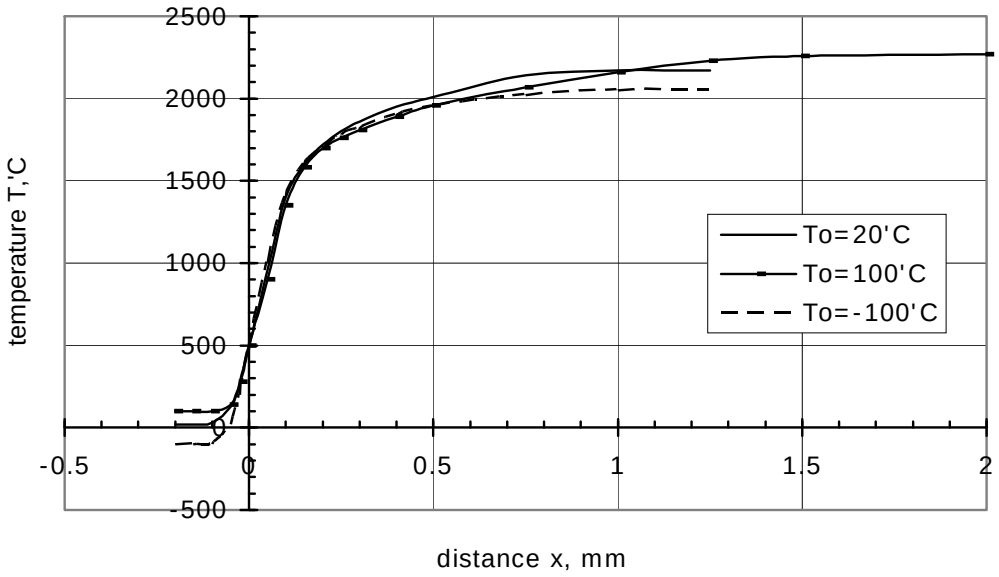

Figure 17: Averaged temperature profiles T(x) of mixture 3 [(BAMO-THF)/HMX, (20:80)] at 10 MPa and various To.

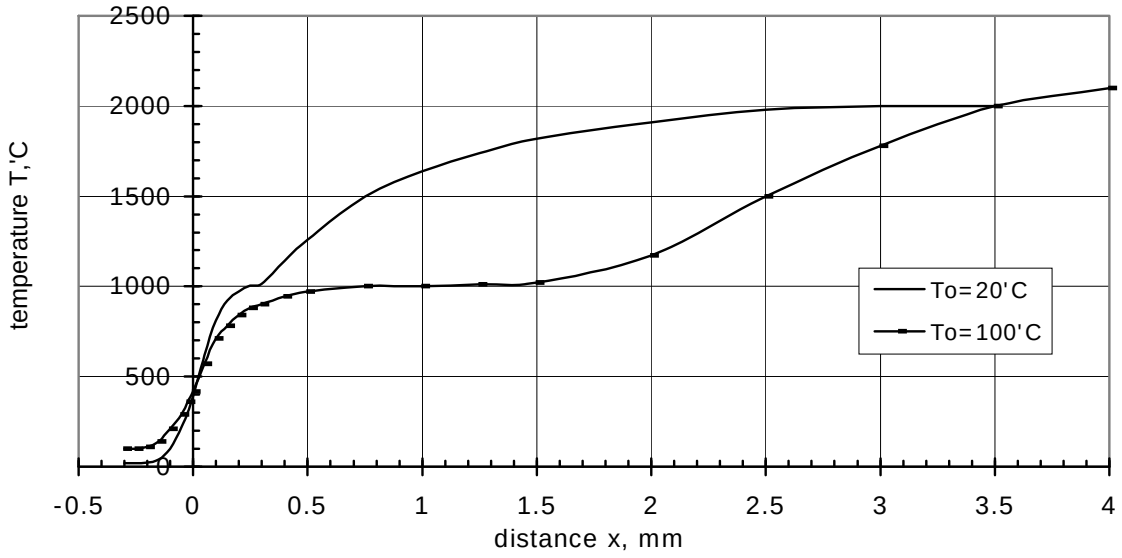

Figure 18: Averaged temperature profiles T(x) of mixture 4 [(BAMO-AMMO)/HMX+stear.Pb, (20:77:3)] at 1 MPa and various To.

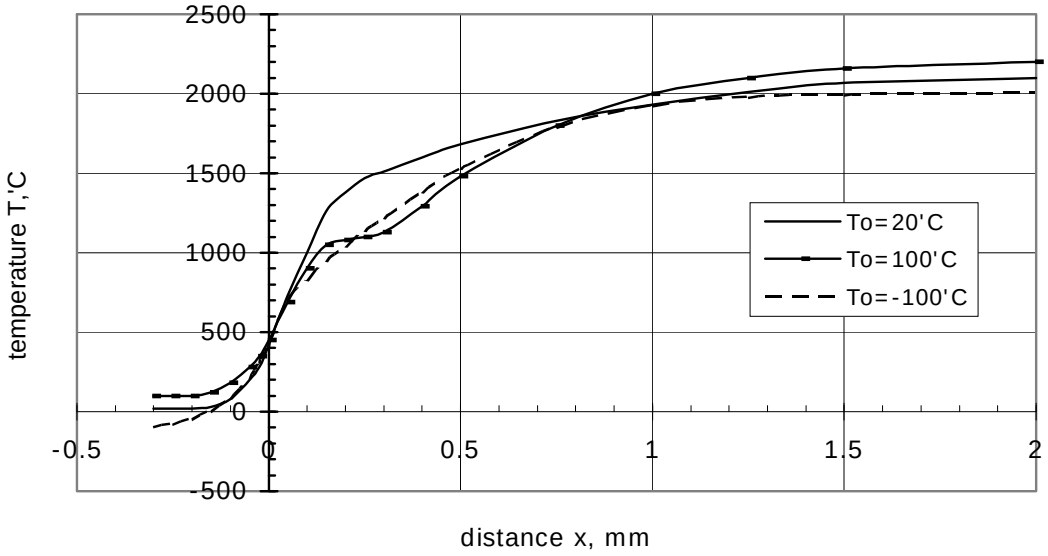

Figure 19: Averaged temperature profiles T(x) of mixture 4 [(BAMO-AMMO)/HMX+stear.Pb, (20:77:3)] at 2 MPa and various To.

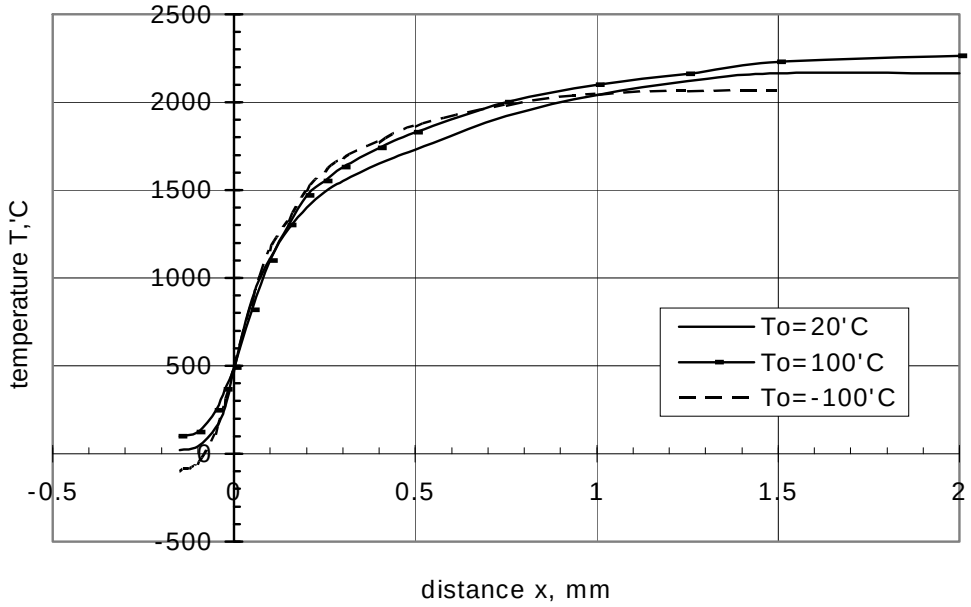

Figure 20: Averaged temperature profiles T(x) of mixture 4 [(BAMO-AMMO)/HMX+stear.Pb, (20:77:3)] at 5 MPa and various To.

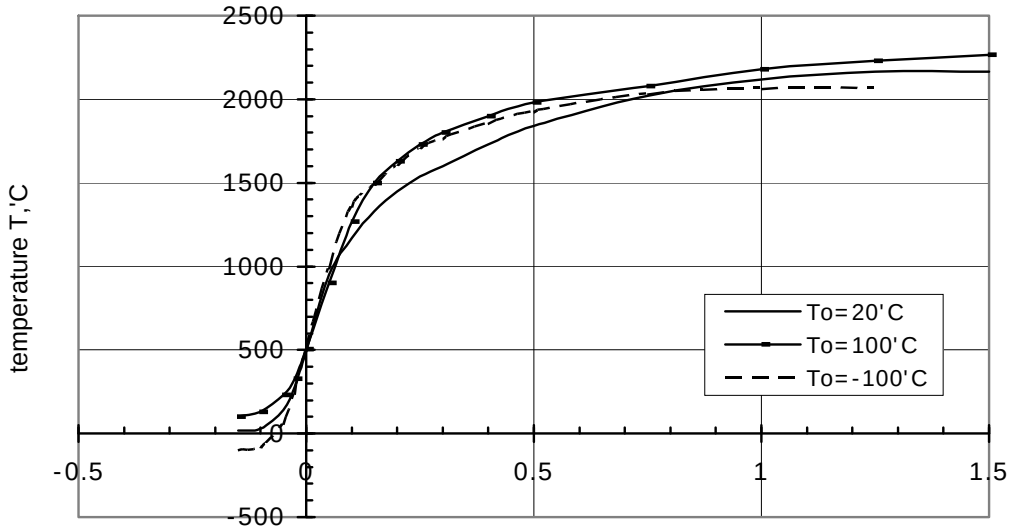

Figure 21: Averaged temperature profiles T(x) of mixture 4 [(BAMO-AMMO)/HMX+stear.Pb, (20:77:3)] at 8 MPa and various To.

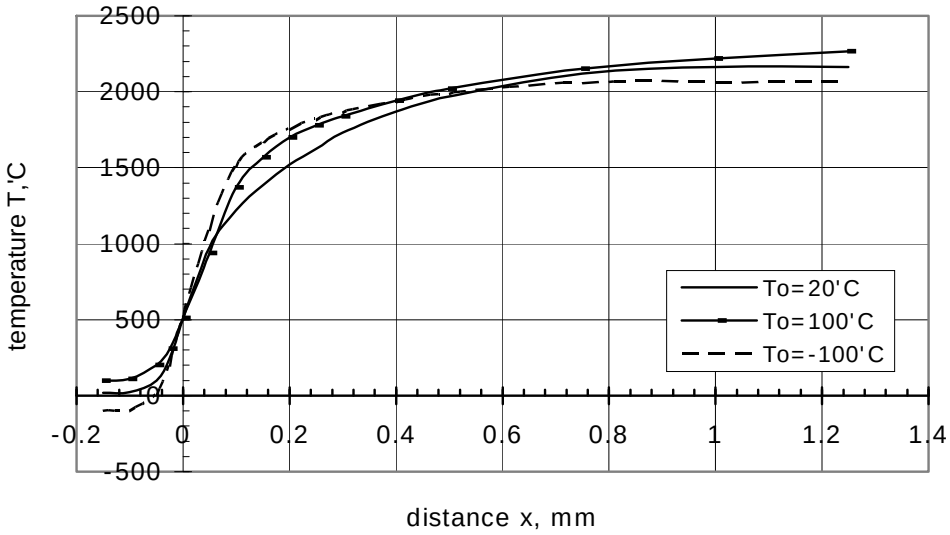

Figure 22: Averaged temperature profiles T(x) of mixture 4 [(BAMO-AMMO)/HMX+stear.Pb, (20:77:3)] at 10 MPa and various To.

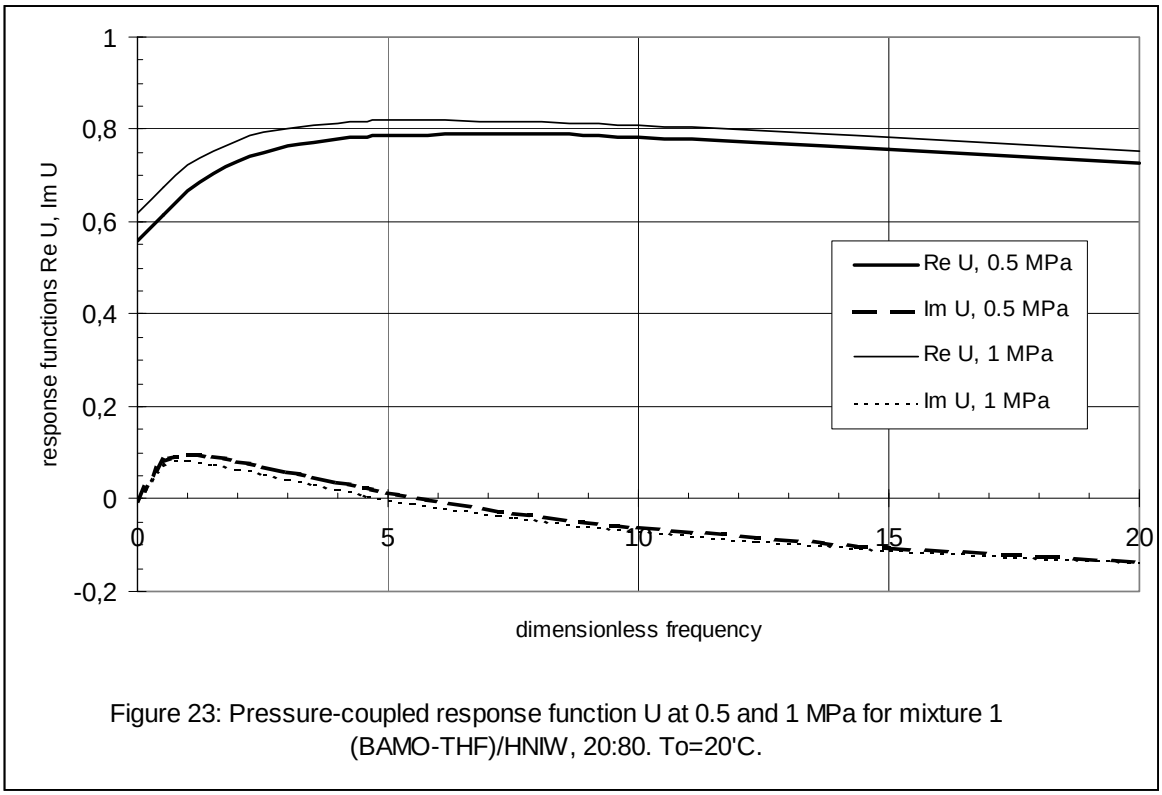

Figure 23: Pressure-coupled response function U at 0.5 and 1 MPa for mixture 1 (BAMO-THF)/HNIW, 20:80. To=20'C.

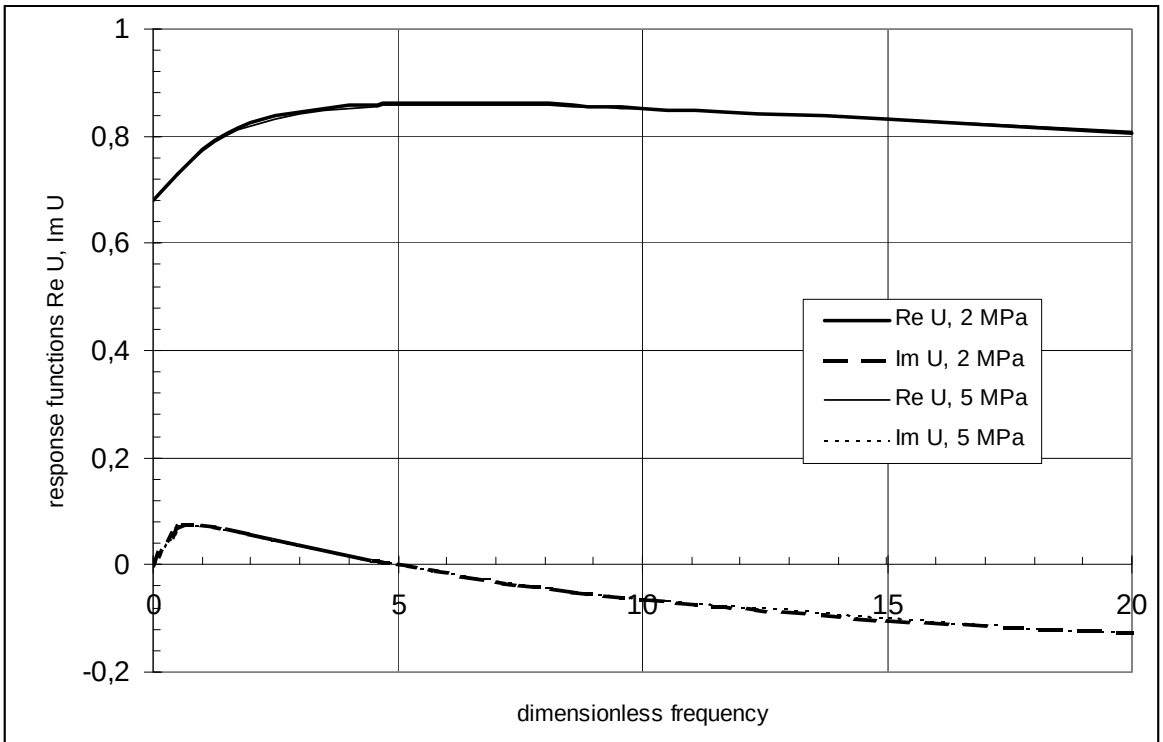

Figure 24: Pressure-coupled response function U at 2 and 5 MPa for mixture 1 (BAMO-THF)/HNIW, 20:80. To=20'C.

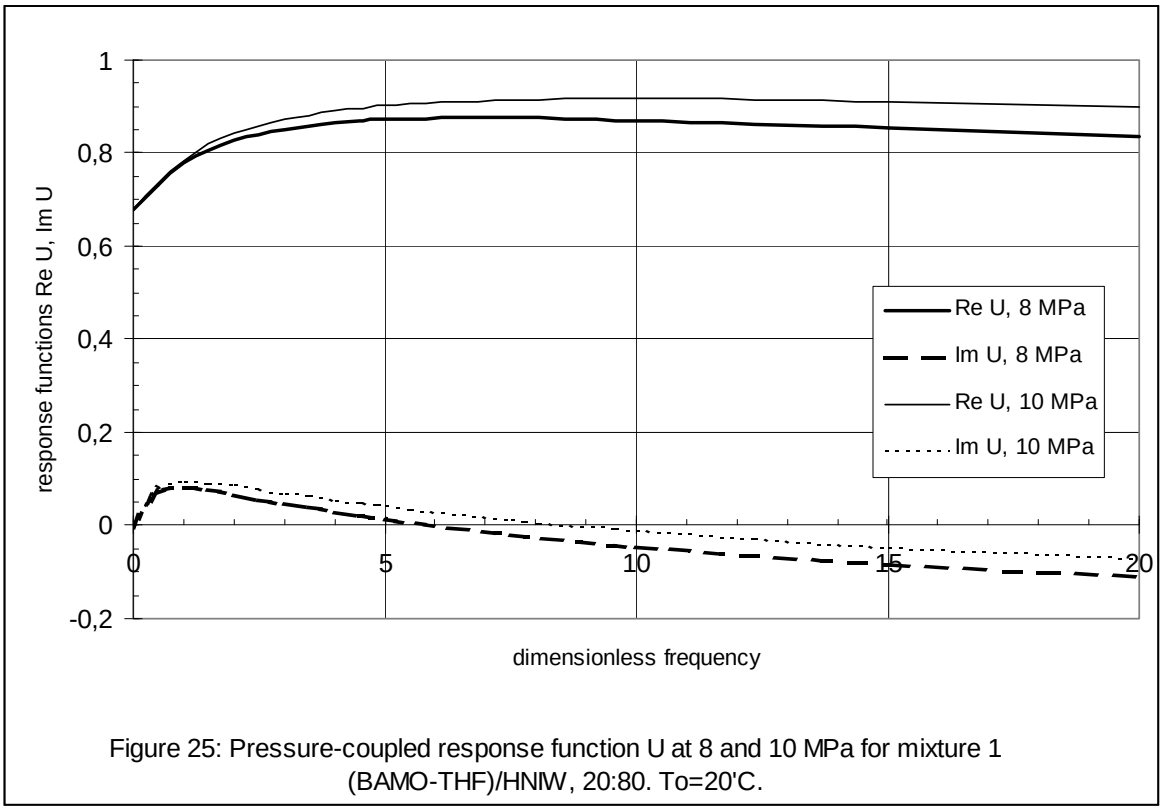

Figure 25: Pressure-coupled response function U at 8 and 10 MPa for mixture 1 (BAMO-THF)/HNIW, 20:80. To=20'C.

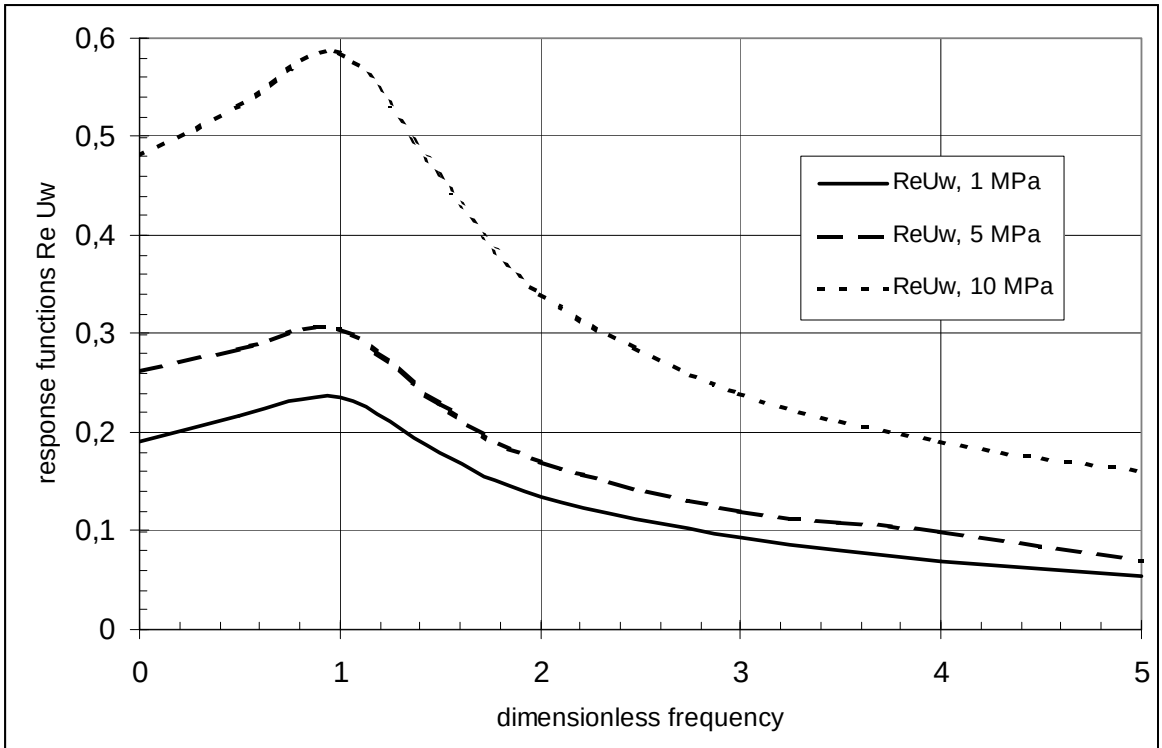

Figure 26: Velocity-coupled burn-rate response functions Re Uw of mixture 1 at 1, 5, and 10 MPa. W=300 m/s. To=20'C.

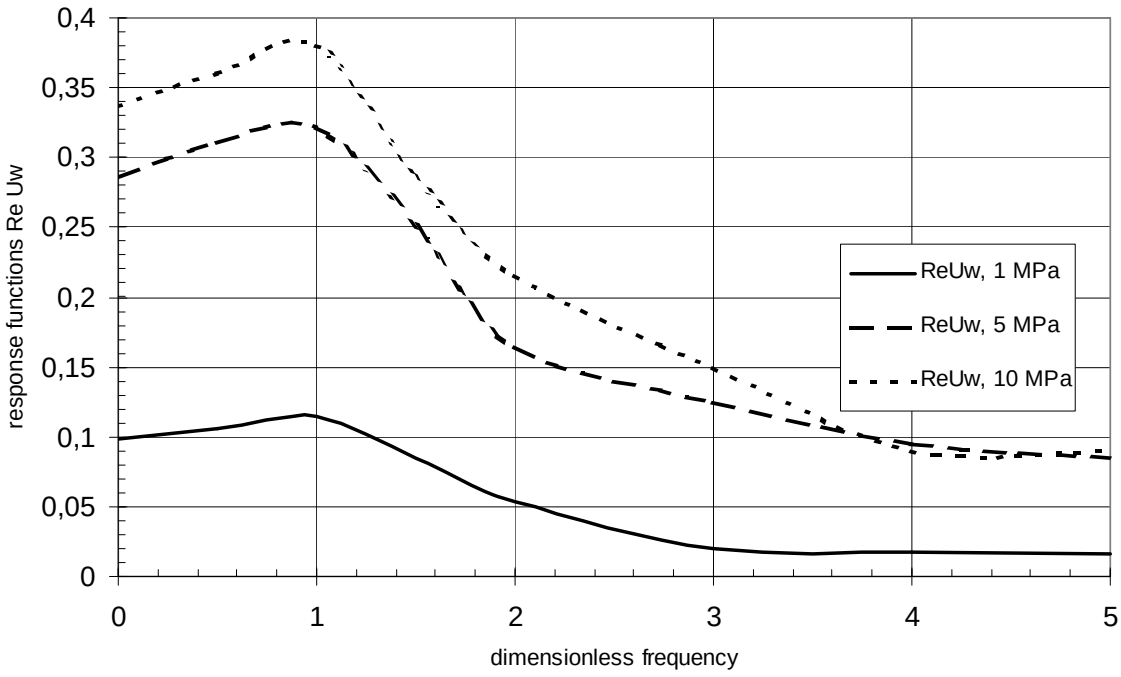

Figure 27: Velocity-coupled burn-rate response functions Re Uw of mixture 2 at 1, 5, and 10 MPa. W=300 m/s.To=20'C.

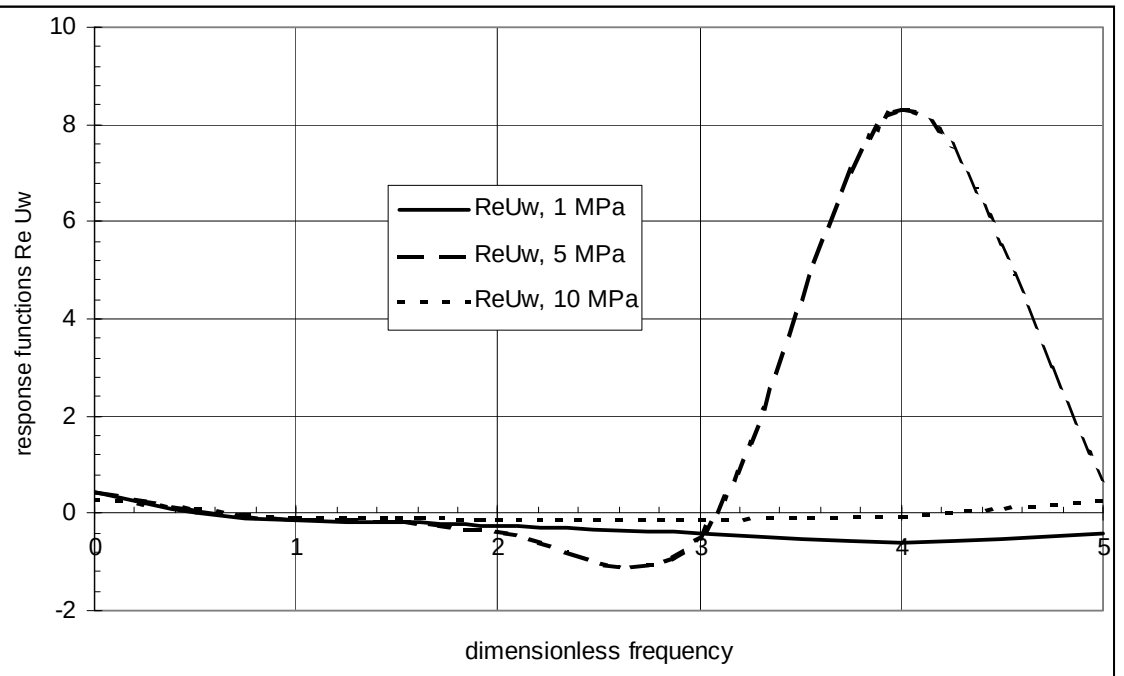

Figure 28: Velocity-coupled burn-rate response functions Re Uw of mixture 3 at 1, 5, and 10 MPa. W=300 m/s.To=20'C.

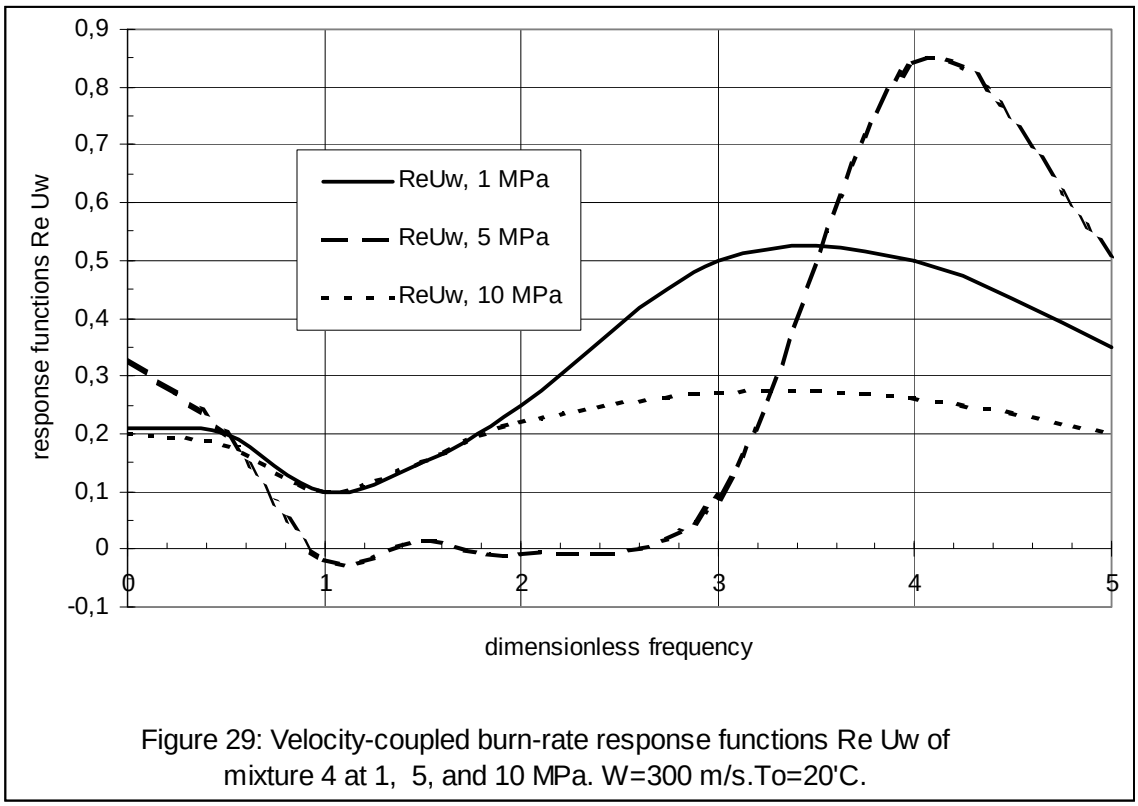

Figure 29: Velocity-coupled burn-rate response functions Re Uw of mixture 4 at 1, 5, and 10 MPa. W=300 m/s.To=20'C.

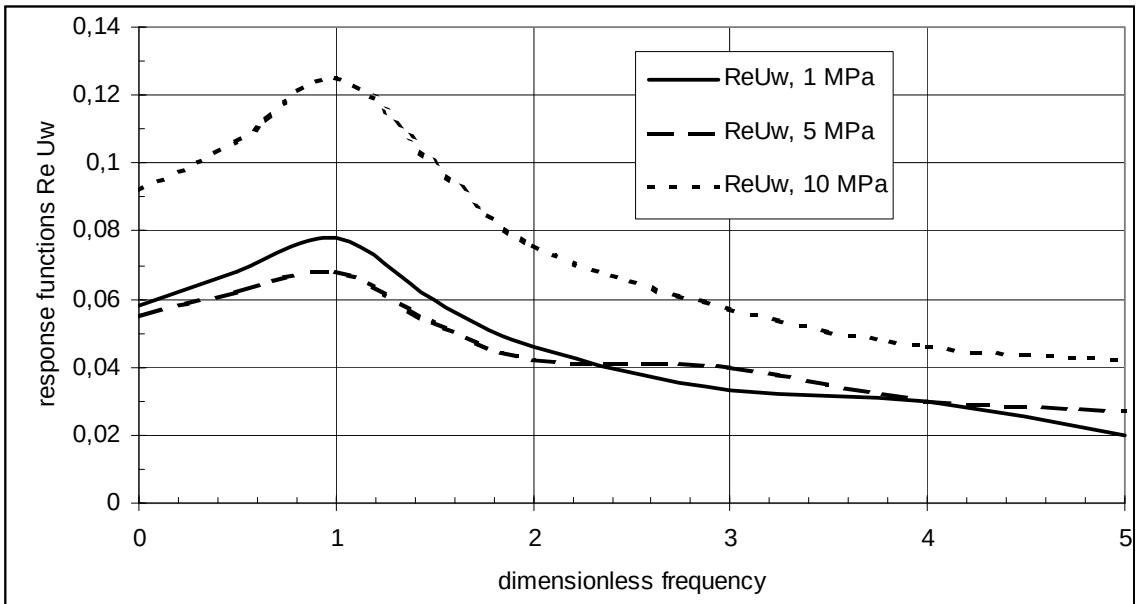

Figure 30: Velocity-coupled burn-rate response functions Re Uw of mixture (AMMO-BAMO)/HNIW, 20:80, at 1, 5, and 10 MPa. W=300 m/s.To=20'C.

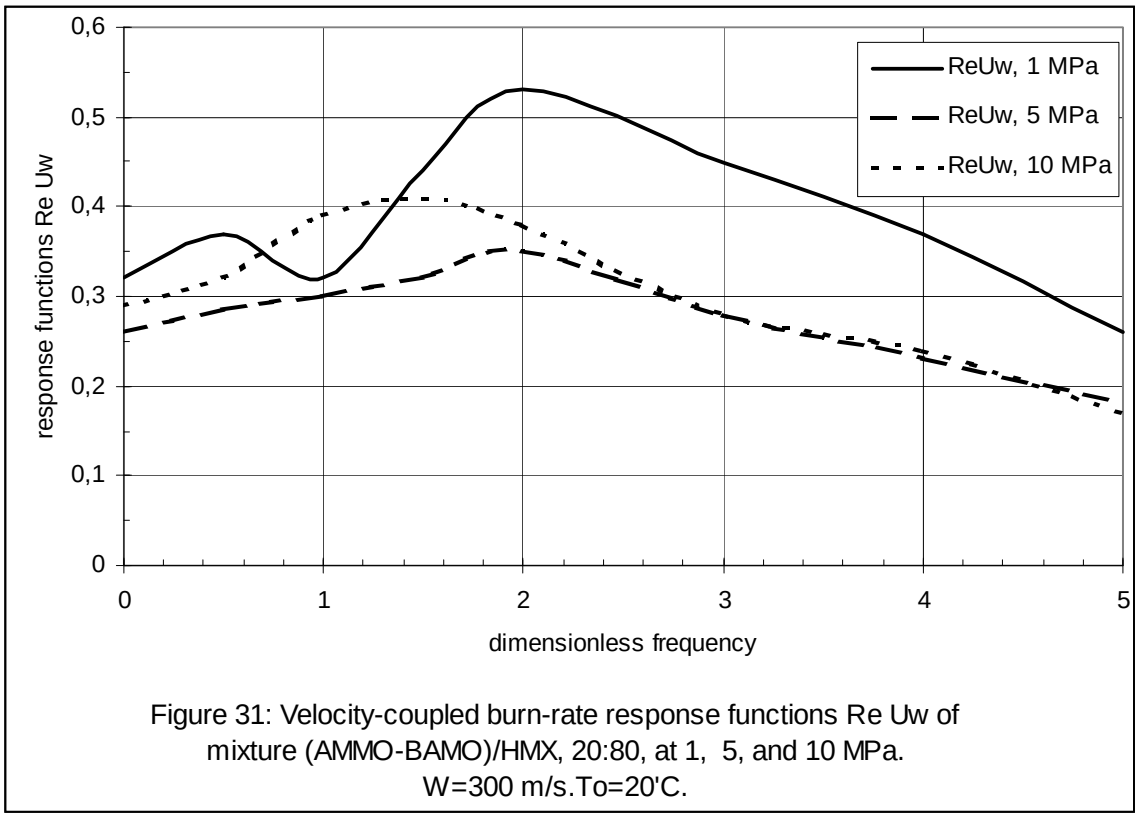

Figure 31: Velocity-coupled burn-rate response functions Re Uw of mixture (AMMO-BAMO)/HMX, 20:80, at 1, 5, and 10 MPa. W=300 m/s.To=20'C.